

Spring 1997

Modeling of the electromagnetic radiation from shielded enclosures with apertures and attached wires in a real-world environment

Bruce Roy Archambeault
University of New Hampshire, Durham

Follow this and additional works at: <https://scholars.unh.edu/dissertation>

Recommended Citation

Archambeault, Bruce Roy, "Modeling of the electromagnetic radiation from shielded enclosures with apertures and attached wires in a real-world environment" (1997). *Doctoral Dissertations*. 1936.
<https://scholars.unh.edu/dissertation/1936>

This Dissertation is brought to you for free and open access by the Student Scholarship at University of New Hampshire Scholars' Repository. It has been accepted for inclusion in Doctoral Dissertations by an authorized administrator of University of New Hampshire Scholars' Repository. For more information, please contact nicole.hentz@unh.edu.

INFORMATION TO USERS

This manuscript has been reproduced from the microfilm master. UMI films the text directly from the original or copy submitted. Thus, some thesis and dissertation copies are in typewriter face, while others may be from any type of computer printer.

The quality of this reproduction is dependent upon the quality of the copy submitted. Broken or indistinct print, colored or poor quality illustrations and photographs, print bleedthrough, substandard margins, and improper alignment can adversely affect reproduction.

In the unlikely event that the author did not send UMI a complete manuscript and there are missing pages, these will be noted. Also, if unauthorized copyright material had to be removed, a note will indicate the deletion.

Oversize materials (e.g., maps, drawings, charts) are reproduced by sectioning the original, beginning at the upper left-hand corner and continuing from left to right in equal sections with small overlaps. Each original is also photographed in one exposure and is included in reduced form at the back of the book.

Photographs included in the original manuscript have been reproduced xerographically in this copy. Higher quality 6" x 9" black and white photographic prints are available for any photographs or illustrations appearing in this copy for an additional charge. Contact UMI directly to order.

UMI

A Bell & Howell Information Company
300 North Zeeb Road, Ann Arbor MI 48106-1346 USA
313/761-4700 800/521-0600

**MODELING OF THE ELECTROMAGNETIC RADIATION
FROM SHIELDED ENCLOSURES WITH APERTURES AND
ATTACHED WIRES
IN A REAL-WORLD ENVIRONMENT**

by

Bruce R. Archambeault

B.S.E.E., University of New Hampshire, June 1977

M.S.E.E., Northeastern University, June 1981

DISSERTATION

Submitted to the University of New Hampshire
Department of Electrical and Computer Engineering
in Partial Fulfillment of the Requirements for the Degree of

Doctor of Philosophy

in

Engineering

May 1997

UMI Number: 9730819

UMI Microform 9730819
Copyright 1997, by UMI Company. All rights reserved.

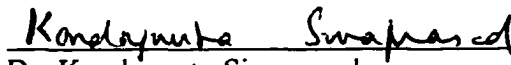
**This microform edition is protected against unauthorized
copying under Title 17, United States Code.**

UMI
300 North Zeeb Road
Ann Arbor, MI 48103

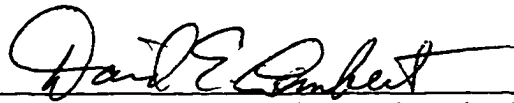
This dissertation has been examined and approved.



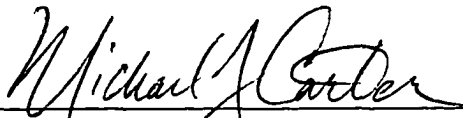
Dissertation Director, Dr. Kent Chamberlin,
Professor of Electrical Engineering



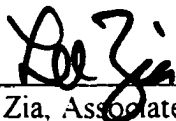
Dr. Kondagunta Sivaprasad,
Professor of Electrical Engineering



Dr. David Limbert, Professor of Mechanical Engineering



Dr. Michael J. Carter,
Associate Professor of Electrical Engineering



Dr. Lee Zia, Associate Professor of Mathematics



Dr. Omar Ramahi, Principal Engineer,
Digital Equipment Corporation

May 13, 1997
Date

DEDICATION

The results of this effort are dedicated to my father, Wilfred Archambeault, who instilled within me the certain knowledge that I can achieve whatever goals I set for myself. Although he was not a famous man, he was the most important man I've ever known.

I also wish to dedicate this to my wife, Sue. Her unflagging confidence that I would succeed and her unselfishness through all the long hours spent on this has helped assure my success.

ACKNOWLEDGMENTS

I would like to acknowledge my friend and colleague, Dr. Omar Ramahi. His advice, support and technical assistance have been invaluable. I doubt I could ever convey the depth of my appreciation.

I would also like to acknowledge the help and support of my advisor, Professor Kent Chamberlin, who allowed me to be an unconventional student and kept me focused on the task at hand.

TABLE OF CONTENTS

| | |
|------------------------------|------------|
| Dedication | iii |
| Acknowledgments | iv |
| List of Figures | ix |
| Abstract | xii |

1 Introduction

| | |
|--|----|
| 1.1 Background | 1 |
| 1.2 Practical EMI/EMC Problem and Test Environment | 3 |
| 1.2.1 Partitioning the Problem into Solvable Modules | 5 |
| 1.3 Description of the Thesis | 8 |
| 1.4 Modeling Techniques | 9 |
| 1.4.1 Finite-Difference Time-Domain Method | 9 |
| 1.4.2 Method of Moments | 10 |
| 1.5 Hybrid Technique | 11 |
| 1.6 General Approach to Developing a Hybrid Model | 11 |

2 Traditional Aperture Modeling Efforts

| | |
|---|----|
| 2.1 Introduction | 13 |
| 2.2 The Surface Equivalence Theorem | 13 |
| 2.3 Closed Form Approaches | 16 |

3 Introduction to the Finite-Difference Time-Domain Technique

| | |
|---|----|
| 3.1 Background | 17 |
| 3.2 The Basis of FDTD | 17 |
| 3.2.1 One Dimensional FDTD | 18 |
| 3.2.2 Two Dimensional FDTD | 20 |
| 3.2.3 Three Dimensional FDTD | 21 |
| 3.3 Stability Conditions | 23 |
| 3.4 Absorbing Radiation Boundary Conditions | 23 |
| 3.5 Summary | 25 |

4 Stage One Model Using FDTD

| | |
|---|----|
| 4.1 Introduction | 26 |
| 4.2 Characterizing Aperture Field Distribution Using FDTD | 26 |
| 4.3 Aperture Impedance | 28 |
| 4.4 Single Aperture Model | 31 |
| 4.4.1 Computational Domain Size | 31 |
| 4.4.2 Aperture Resonant Frequency | 33 |
| 4.4.3 Source Position and Illumination Angle | 34 |
| 4.4.4 Source Distance from Aperture | 36 |
| 4.4.5 Impedance Variation Along the Aperture | 38 |
| 4.4.6 FDTD Impedance Anomalities | 40 |

| | |
|---|----|
| 4.5 Multiple Apertures | 40 |
| 4.6 Summary | 43 |
| 5 Correcting the Electric Fields within the Aperture at Low Frequencies | |
| 5.1 Introduction | 44 |
| 5.2 Using the Herzian Dipole Impedance Technique to Correct the Low Frequency Aperture Impedance | 46 |
| 5.3 Correcting the Electric Fields in the Aperture at Low Frequencies | 50 |
| 5.4 Summary | 50 |
| 6 Introduction to the Method of Moments Technique | |
| 6.1 Background | 52 |
| 6.2 The Basics of MoM | 53 |
| 6.3 Filling the Impedance Matrix | 56 |
| 6.4 Finding the Electric Fields from the RF Currents | 59 |
| 6.5 Summary | 60 |
| 7 Hybrid Technique Stage Two Modeling Using MoM | |
| 7.1 Introduction | 61 |
| 7.2 Initial Aperture Models | 62 |
| 7.2.1 Single Aperture MoM Model | 62 |
| 7.2.2 Double Aperture MoM Model | 66 |

| | |
|---|----|
| 7.3 Summary | 68 |
| 8 Implementing the Hybrid Technique | |
| 8.1 Introduction | 70 |
| 8.2 Detailed Description of the Hybrid Technique | 70 |
| 8.3 Enclosed Shielded Enclosure with Aperture Model | 72 |
| 8.3.1 Hybrid Model Comparison Between Free Space and Real-World Test Environment | 73 |
| 8.4 Summary | 76 |
| 9 Summary | 73 |
| 10 References | 76 |
| Appendix A Additional Aperture Size Characterization | 79 |

LIST OF FIGURES

| | |
|---|----|
| Figure 1.1 Real World EMI Emissions Test Environment | 6 |
| Figure 2.1 Equivalent Models for Aperture in Infinite Plate | 15 |
| Figure 3.1 One Dimensional FDTD Grid | 19 |
| Figure 3.2 Two Dimensional FDTD Grid | 20 |
| Figure 3.3 Three Dimensional FDTD Cell | 22 |
| Figure 4.1 Single Aperture in Infinite Conducting Sheet | 27 |
| Figure 4.2 FDTD Model for Single Aperture in Infinite Metal Sheet | 28 |
| Figure 4.3 Typical Aperture Impedance vs. Frequency | 29 |
| Figure 4.4 Typical Aperture Impedance Along Aperture | 30 |
| Figure 4.5 FDTD Model for Single Aperture with Different Computational Domain Sizes | 32 |
| Figure 4.6 Impedance Variation in Aperture Center Due to White Space Above Aperture (10x4 mm Aperture) | 33 |
| Figure 4.7 Aperture Impedance Variation Due to White Space for 20x2 mm Aperture | 34 |
| Figure 4.8 Z_{xy} Impedance at Center of 10x2 mm Aperture | 35 |
| Figure 4.9 Aperture First Resonant Frequency for Different Size Apertures | 35 |
| Figure 4.10 Aperture Impedance Due to Source Illumination Angle (10x2 mm) | 36 |
| Figure 4.11 Effect of Source Distance on Aperture Impedance Z_{xy} for 10x2 mm Aperture (center)..... | 37 |
| Figure 4.12 Variation of Impedance (Z_{xy}) Across Aperture (10x2 mm) | 39 |

| | |
|---|----|
| Figure 4.13 Maximum Impedance Z_{xy} (at First Resonant Frequency) for Various Aperture Sizes..... | 39 |
| Figure 4.14 Dual Aperture Configuration | 41 |
| Figure 4.15 Impedance (Z_{xy}) Across Aperture (10x2 mm) (First Slot of Dual Slot Configuration) | 42 |
| Figure 4.16 Variation of Impedance (Z_{xy}) Across Aperture (10x2 mm) (First Slot of Dual Slot Configuration)..... | 42 |
| Figure 5.1 Comparison of Predicted and FDTD Aperture Impedance | 48 |
| Figure 5.2 Original Impedance for 20x2 mm Aperture | 48 |
| Figure 5.3 Original FDTD and Predicted Aperture Impedance for 20x2 mm Aperture | 49 |
| Figure 5.4 Original FDTD and Predicted Electric Field Level in Aperture for 20x2 mm Aperture | 51 |
| Figure 6.1 MoM Geometry for Current on a Wire Segment | 55 |
| Figure 7.1 MoM Wire Frame Model with Single 10x2 mm Aperture | 63 |
| Figure 7.2 Electric Field Distribution from MoM Model for 10x2 mm Aperture | 65 |
| Figure 7.3 Comparison Between MoM and FDTD at 65mm from Single Aperture | 65 |
| Figure 7.4 MoM Wire Frame Model with Two 10x2 mm Apertures | 67 |

| | |
|---|----|
| Figure 7.5 Comparison Between MoM and FDTD at 65mm from Two Apertures | 68 |
| Figure 8.1 FDTD Example Model of Shielded Enclosure with Aperture Model | 72 |
| Figure 8.2 MoM Wire Frame Enclosure Model | 73 |
| Figure 8.3 Maximized Electric Field Comparison with and without Ground Plane (Horizontal)..... | 74 |
| Figure 8.4 Maximized Electric Field Comparison with and without Ground Plane (Vertical)..... | 75 |
| Figure 8.5 MoM Model of Shielded Enclosure with 1 Meter Cable | 76 |
| Figure 8.6 Maximum Received Electric Field from EUT with One Meter Wire Attached | 77 |
| Figure A-1 Z_{xy} Impedance at Center of 5x2 mm Aperture | 85 |
| Figure A-2 Z_{xy} Impedance at Center of 15x2 mm Aperture..... | 85 |
| Figure A-3 Z_{xy} Impedance at Center of 20x2 mm Aperture | 86 |
| Figure A-4 Z_{xy} Impedance at Center of 25x2 mm Aperture | 86 |
| Figure A-5 Variation of Impedance (Z_{xy}) Across Aperture (5x2 mm) | 87 |
| Figure A-6 Variation of Impedance (Z_{xy}) Across Aperture (20x2 mm) | 87 |

ABSTRACT

MODELING OF THE ELECTROMAGNETIC RADIATION FROM SHIELDED ENCLOSURES WITH APERTURES AND ATTACHED WIRES IN A REAL-WORLD ENVIRONMENT

by

Bruce Archambeault
University of New Hampshire, May 1997

A hybrid modeling technique using the Finite-Difference Time-Domain (FDTD) approach in conjunction with the Method of Moments (MoM) approach was developed to allow simulation of electromagnetic interference (EMI) emissions through apertures due to sources within a shielded enclosure. These apertures can include air ventilation openings, option card slots, mating cover seams, or any other opening in the metal shielded enclosure. Modeled emission results can now be directly compared to U.S. and other countries' regulations to allow engineers to predict compliance before hardware prototypes are built. The effects of the test environment, including ground plane and specified measurement distance, as well as configuration requirements, such as long attached wires, are included and result in more accurate models of the real-world environment than previously possible.

The first stage of the hybrid technique uses the FDTD approach to model the source within the shielded enclosure and to find the electric fields within the aperture or apertures. The sources within the enclosure include printed circuit board traces, internal wires and cables, and discrete devices, such as integrated circuits and heatsinks. Errors in the aperture fields at low frequencies due to limitations in the FDTD absorbing boundary conditions are then corrected using an extrapolation technique. Once the electric fields within the aperture are known, they become the source for the second stage of the hybrid technique. This second stage uses MoM to find the external fields while including the effects of long attached wires, ground planes, and a distant receive location. The results from the second stage can then be compared to the various regulatory agency requirements.

CHAPTER 1

INTRODUCTION

1.1 Background

In 1981, the Federal Communications Commission (FCC) established limits on the strength of electromagnetic radiation allowable from computing devices sold in the United States. [1] In the past few years, various other countries have developed similar standards, mostly to control these devices' potential to interfere with data communications systems, broadcast radio and television, and emergency systems. The European Community has recently standardized these requirements in Europe, and expanded them to include not only computing devices, but nearly every product containing digital electronics [2].

The result of these various regulations is that all manufacturers, not only computer manufacturers, must pay close attention to the electromagnetic interference (EMI) levels that their products produce. Pressures to shorten design cycle times, reduce product costs, and meet EMI regulations has served to increase the interest in using modeling and simulation to help ensure optimum hardware designs. An optimum design will ensure only required EMI features are included, since it is no longer acceptable in industry to simply use excessive shielding, costly filters, small aperture air vents, and other such fixes to meet EMI regulations.

If sufficient computer resources (memory and speed) were available, the entire problem could be modeled using the Finite-Difference Time-Domain (FDTD) approach. Unfortunately, due to limits in computer speed and memory, present modeling capabilities are not even close to the point where a complete design layout can be entered into a EMI modeling application, all the various components included, and a pass/fail estimate be obtained. However, modeling and simulation have been used in the past for specific aspects of the overall problem, such as shielding of apertures and slots, radiation from cables, and radiation from simple printed circuit boards. Although these various models can help the EMI engineer by providing additional understanding into the nature of the electromagnetic phenomena, it often gives too little information about the overall system performance to be used in assessing whether or not the final product will pass the emissions requirements.

Typically, electromagnetic radiation testing is performed as a *system*, that is, all the various parts that are generally used together must be tested together. In the case of a most personal computers, this would include the computer system box, monitor, keyboard, mouse, and printer. Also, any other cables that might be connected to the units must be included, for example, modem cables, speaker cables, etc.

Measurements to test for regulatory compliance are performed over a ground reference plane, with all the equipment placed on a wood table 80 cm high. The radiated emissions are measured at a distance 10 meters away from the equipment under test (EUT) while it is rotated 360 degrees and the receive antenna is scanned vertically from one to four meters above the ground reference plane. [1][2] All interconnecting cables for the device being measured are to be positioned for maximum radiation. Results generated by existing models have been of limited use because they have not been able to effectively account for cables or the test environment. Consequently, these models

have not been able to provide crucial pass/fail estimates of equipment performance against the regulatory standards.

The work presented here focuses on modeling the entire problem, that is, the radiation from a source within a shielded enclosure, the coupling of that energy to the outside via apertures in the enclosure, the effect of wires connected nearby those apertures, and the test environment itself. Because of the complex nature of the problem, it is impractical to accurately model this problem without using multiple modeling stages and different modeling approaches. The method to be presented here makes possible the modeling of configurations that were previously considered impractical. This method also makes possible direct comparisons of the simulation results to the regulatory limits to predict pass/fail of the device.

1.2 Practical EMI/EMC Problem and Test Environment

Although there is a large number of different types of products that must meet EMI/EMC regulations, most fall into the general class of products with shielded enclosures containing apertures and having long wires attached to the enclosure¹. Plastic enclosures are often shielded either by a metal internal coating or by metal fragments imbedded in the plastic during the molding process. Computer products, consumer electronics products, and communications devices all fit this category:

¹ Note: the attached wires are assumed to be connected to the enclosure shield, and are not in the aperture itself. Although wiring connectors can be modeled as an aperture with a wire through it, experience has shown that conducted emissions along the wire/connector are a more important concern in those cases. This effort focuses on radiation through apertures (without wires). Since all exiting wires are intentionally capacitively decoupled to the shielded enclosure for EMI control reasons, they can be modeled as being physically connected to the shielded enclosure.

The source of the radiated emissions is usually a high speed (fast rise time) clock or data signal on the printed circuit board within the shielded enclosure. The source creates a complex electric and magnetic field structure within the enclosure. Some of this energy 'leaks' out through the apertures (e.g. air vents, slots between option cards, shielded enclosure seams) and creates RF currents on the outside of the shielded enclosure. These currents are then distributed over the entire outside structure (including wires, cables, etc.), and radiate into the outside environment. The fields are then measured 10 meters away in the presence of a ground reference plane, as described earlier.

The products under test typically have long wires attached to different connectors (power cords, modem lines, printer cables, etc.) which will greatly affect the radiated emissions from the product. RF currents that have leaked out from an aperture and are on the outside of the metal shield will couple onto the wires and cables. The wires will greatly increase the effective aperture of the 'antenna' (the equipment under test or EUT) since the overall size of the EUT with wires is typically increased by more than an order of magnitude by the presence of the wires. Experience has shown that products without attached cables and wires can more readily achieve EMI regulatory compliance. The test standards require that every type of port/interface must be connected to the correct cable or wire, and the cables and wires must be positioned to ensure maximum radiated emissions. Furthermore, the EUT must include all equipment typically included in system configurations (e.g. computer, printer, keyboard, mouse, monitor, etc.). Figure 1.1 shows a typical example of such a computer product with cables. This is a difficult modeling task. Including the test environment makes this modeling task even more difficult because the interaction between the ground reference plane and the EUT must be taken into account.

1.2.1 Partitioning the Problem into Solvable Modules

Using contemporary computational technology and techniques, there is no practical way to model the entire problem described above with a single model. Earlier work has been performed that successfully models certain aspects of the overall problem, (e.g. radiation from printed circuit boards (PCB) with a microstrip near a reference plane edge [3][4], PCB via's [4], decoupling capacitor placement [5], or shielding through apertures [6][7][8][9][10]), but because these efforts have addressed only specific facets of the overall problem, they were not adequate to predict compliance with regulatory standards. For example, in both [3] and [4], emissions from an unshielded printed circuit board (PCB) with a microstrip was modeled. No attempt to include a shielded enclosure with apertures was made. In [6][7][8][9][10] emissions through apertures in a infinite metal sheet were modeled, but no attempt was made in these previous studies to include a PCB as the source, nor to include the required measurement environment. These studies were useful to help understand specific phenomena, but did not include all the parts of the overall problem to allow for comparison to the regulatory limits.

The focus of this dissertation is the development of a hybrid technique to model much more of the overall problem than has been previously possible. The strengths of the two modeling approaches implemented in the hybrid technique allow a source, a shielded enclosure with apertures, and the required measurement environment. Thus the results of the overall problem can now be compared to the regulatory limits for pass/fail analysis. Other internal features, such as partial shielding walls, extra cables, etc. can be included as required. This hybrid technique uses the Finite-Difference Time-Domain (FDTD) method to model the source and the inside of the shielded

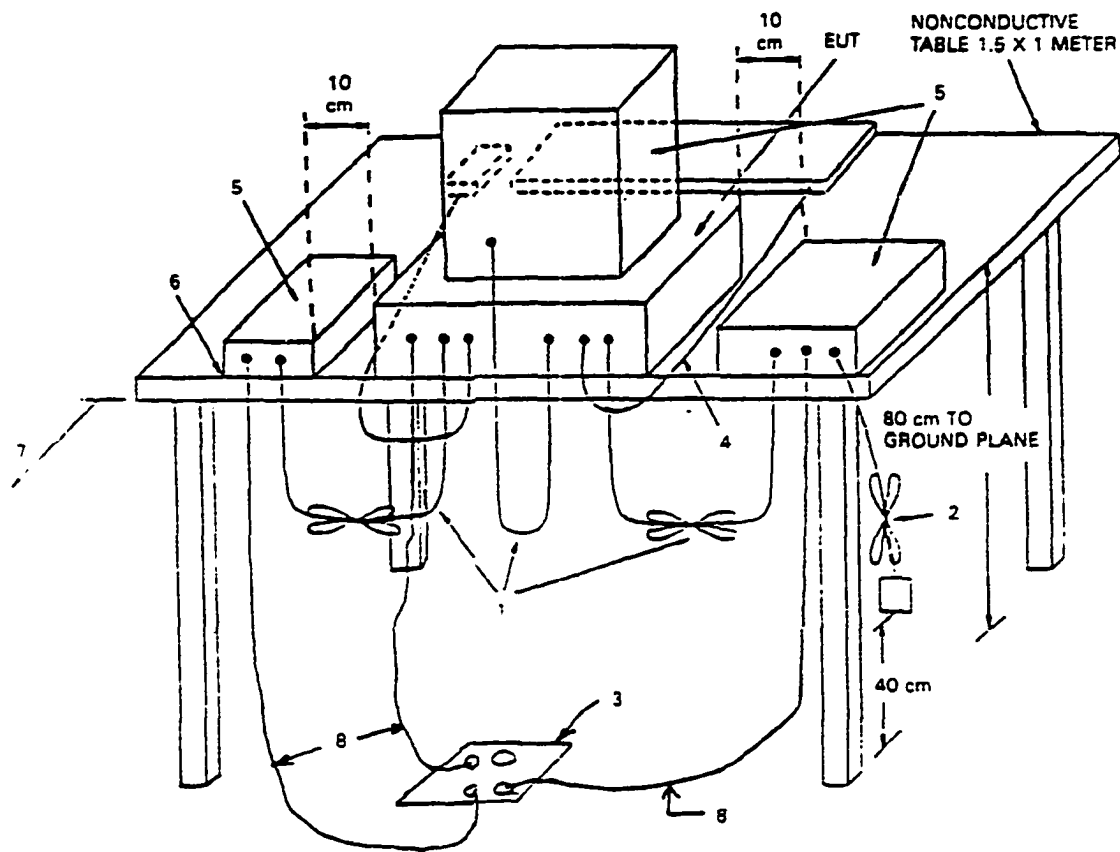


Figure 1. 1 Real World EMI Emissions Test Environment

enclosure, including the effects of the apertures. The Method of Moments (MoM) approach is used to model the outside of the shielded enclosure, including attached wires, and the test environment.

Modeling the source within the enclosure is a difficult problem. Due to memory and processor speed limitations in contemporary computers, approximations must be made when modeling components within the enclosure. The high speed traces, bus traces, or CPU heatsinks are typically considered the most important EMI sources, and are modeled as relatively simple wire

sources (without all the detail of the true printed circuit board). Depending upon the design, separate models might be used to determine the primary emission sources on a printed circuit board, and then the circuit board is reduced to a simple model with only that source. In order to demonstrate this technique, a PCB edge is assumed to be in close proximity to an enclosure aperture. It has been shown [3] that RF currents along an edge of a PCB reference plane due to microstrip or stripline currents are equivalent to a thin wire (replacing the PCB edge) with a dipole-like current distribution. This is assumed to be the worst case EMI source, but other sources can also be used. The hybrid technique is not dependent on a given source type. The power of this technique allows sources to be modeled as needed. In this dissertation, a simple wire with a current on it is used as the initial source. Simplifying the complex PCB source into a wire with a current has been shown through practical use to provide good first-order results [3][11][12].

Once the source model has been developed, the next problem is to correctly model the amount of energy leaking through the apertures in the shielded enclosure due to the fields within the shielded enclosure. For example, the rear panel of a computer enclosure typically has openings which appear as large electromagnetic apertures, often 10 cm long with wires attached nearby.

In order to achieve the necessary model accuracy, it is not sufficient to model the aperture alone, or even an aperture with a wire in close proximity, but the complete test environment must be included as well. Although Figure 1.1 shows a number of different interconnected shielded enclosures, single enclosure products are often tested alone. For the purposes of this study, the problem in Figure 1.1 is restricted to a single shielded box, with apertures and wires attached to the enclosure, placed over a ground plane, with the measuring antenna 10 meters away. The intent here is to demonstrate that the hybrid model can be used to effectively model leakage through apertures in an enclosure in the presence of the standard test environment. The cases presented here are

intentionally canonic in nature, although in practice more-complex configurations involving multiple enclosures can be modeled using this technique.

1.3 Description of the Thesis

This work is divided into four parts. The first part of this dissertation, contained in Chapters 1 and 2, is devoted to examining the problem to be solved, the various modeling approaches available, and their limitations when applied to this problem. Chapter 1 describes the real-world application, and evaluates the basic strengths and limitations of each different modeling approach in this basic application. Chapter 2 presents a short discussion on previous modeling efforts for apertures.

The second part of the dissertation, (Chapters 3 through 5), is devoted to the FDTD approach. FDTD is used as the 'first stage' modeling approach. That is, it is used to find the electromagnetic fields within the aperture(s) due to a source within the shielded enclosure. This first stage models the inside of the enclosure, including the source and the aperture(s) and can include the complex internal structure, if desired. Fields in the aperture(s) are used later in the Stage Two models to find the fields outside the enclosure. Chapter 3 serves as an introduction to the FDTD approach, including limitations due to the Absorbing Boundary Conditions (ABC) used by FDTD. Chapter 4 shows the results of a study of aperture(s) using FDTD. Chapter 5 discusses techniques to compensate for errors in the fields within the aperture which may occur at low frequencies when certain constraints are violated in the FDTD approach (and therefore is of interest for many EMC applications).

The third part of the thesis, Chapter 6, describes the MoM approach. The MoM approach is used as the second stage modeling technique. It is used to find the electromagnetic fields outside the

enclosure (including long wires attached and over a ground plane, etc.) due to the electromagnetic field within the aperture(s). Chapter 6 serves as an introduction to MoM and its application to modeling enclosures.

In the fourth and final part of the dissertation, Chapter 7 validates the use of the simplified source used in the stage two MoM aperture models by comparing results from similar FDTD models.

Chapter 8 gives a detailed description of how to apply this hybrid technique to aperture problems for users who wish to implement this hybrid technique. An example is given which presents the entire hybrid model, where the inside of the enclosure is modeled using FDTD, and the outside of the enclosure is modeled using MoM. Results are presented for increasingly complex configurations thus demonstrating the utility of this hybrid approach.

1.4 Modeling Approaches

There is no closed-form solution technique which can solve the problem described above, leaving numerical approaches as the only practical solution approach. Two proven methods are the MoM approach and the FDTD approach. Each of these approaches are briefly described here as an introduction to their theory of operation. Greater detail in each modeling approach is given in Chapters 3 and 6.

1.4.1 The Finite-Difference Time-Domain (FDTD) Method

The FDTD approach has become very popular over the last 10 years for EMI applications. FDTD is a volume-based approach, where the volume of space containing the problem is partitioned into small cubes, and Maxwell's equations are solved directly using a central difference scheme. (See Chapter 3 for more details.) The electric and magnetic fields are solved directly using a leapfrog

approach, where the field components are offset in time and space to ensure greater accuracy in approximating their derivatives.

FDTD is well suited for shielding applications with apertures. However, it is not practical for applications with long wires (long with respect to the wavelength), or applications with long distances between the source and the measurement location because of the amount of computer memory required. Since the entire volume must be partitioned into small cells, the memory requirements would far exceed contemporary computer resources if long wires or long distances were to be included.

Part of the overall problem can be modeled using FDTD; FDTD will be used to model the source inside the enclosure and to find the fields in the aperture due to the source inside the enclosure. The inside of the enclosure can be as complex as necessary, and can include partial internal shielding walls, compartments, and whatever other features are important.

1.4.2 Method of Moments

The Method of Moments is a commonly used frequency-domain approach whereby the RF currents are found everywhere on a metal structure due to a specified source (see Chapter 6 for more details). Once the currents are known, the radiated fields can be found by summing the contribution from each current element. Since only the external structure is modeled (rather than gridding all the volume around the shielded box, as with FDTD), MoM is very useful for applications with long wires. MoM is also very useful for applications with appreciable distances to the observation point. However, MoM is not appropriate for problems involving leakage through apertures, since the currents are assumed to be constant everywhere on the segments, which is not

true in cases with metal shields (the current on the outside is different than the current on the inside).

MoM is useful for modeling sources within the aperture and so part of this problem can be modeled using MoM. The long wires on the outside of the shielded box, and the measurement distance of 10 meters can be readily included in MoM. However, the leakage through the aperture(s) can not be modeled in MoM.

1.5 Hybrid Technique

Because no single modeling technique can be used to solve the entire problem, a hybrid technique is required. In the hybrid technique addressed here, both the FDTD and MoM approaches are used. These two approaches have been successfully used together in the past for shielded-cable problems [13], but did not include shielded enclosures, or long measurement distances. In this work, the FDTD approach is used to model the source within the shielded box and the fields in the aperture. The fields in the aperture (found by FDTD) are then used as a source for the external model, which is a MoM model accounting for the effect of extra wires, the presence of a ground plane and long measurement distances.

1.6 General Approach to Developing a Hybrid Model

In developing the hybrid model presented here, a number of studies were performed to ensure that neither FDTD nor MoM produced anomalous results when modeling apertures. The first such study was to investigate how well FDTD modeled fields in an aperture, and to determine the sensitivity of modeled field distribution to source distance, illumination angle, and the presence of other apertures. That investigation, presented in Chapter 4, shows that the fields in the aperture

are relatively insensitive to variations in the aforementioned parameters provided that frequencies are at or below the first resonance frequency of the aperture. This constraint should not pose a limitation for most EMC applications since the first resonance of most enclosure openings are typically well above frequencies that are present in contemporary devices.

That first study also showed that FDTD can induce errors at lower frequencies when the distance in wavelengths from the aperture to the absorbing boundary condition becomes small. A simple theoretical means for compensating for this error is presented in Chapter 5.

Since MoM is used to model fields on the outside of the enclosure in the hybrid model, another study was performed to verify that MoM-modeled fields in the aperture are the same as FDTD-modeled fields in the aperture. As expected, the field distribution in the aperture was nearly identical for both models, indicating that the hybrid approach is viable. This finding is used to facilitate the implementation of the hybrid technique. Specifically, the FDTD modeled electric field in the center of an aperture, determined in the first stage of the hybrid model, is used as the excitation source in the center of the aperture for the MoM model in the second stage. This simplifies the modeling process, since only the field values at one location needs to be stored for each aperture in the problem space. Details of this implementation are given in Chapter 8.

CHAPTER 2

TRADITIONAL APERTURE MODELING EFFORTS

2.1 Introduction

Apertures in metal shields have created an EMI problem since they are a primary means by which interference can leave an enclosure. The analysis of the amount of electromagnetic fields leaking through the apertures has been the subject of study ever since the wavelength of the clock frequencies and its harmonics have approached the size of the enclosure apertures. This chapter will present a brief review of the traditional approach to calculating the shielding effects of these apertures.

2.2 The Surface Equivalence Theorem

The surface equivalence theorem [14] is probably the best known and most commonly used general approach for determining emissions from apertures. It represents the actual source (for example, an antenna and a transmitter) by replacing it with equivalent sources. These new sources are said to be equivalent within a region since they produce the same fields as the actual sources within that region. The surface equivalent theorem is based on the uniqueness theorem which states that "a field in a lossy region is uniquely specified by the sources within the region plus the tangential components of the electric field over the boundary, or the tangential components of the magnetic field over the boundary, or the former over part of the boundary and the latter over the rest of the boundary." [15]

The fields radiating through an aperture in an enclosure may be calculated by placing suitable electric and magnetic currents over the entire surface, satisfying the boundary condition requirement of the tangential electric field equals zero along perfect conductors. The currents on an imaginary closed surface are selected so the fields inside the closed surface (box) are zero (thus exactly matching the tangential fields at the closed surface) and the fields outside the closed surface are the same as those created by the actual sources within the closed surface. Thus this technique can be used to find the fields radiated outside an enclosure by sources inside the enclosure.

To use the approach, the tangential fields must be known in the aperture. This is fairly straightforward when a plane wave is the source, or in the case of a waveguide structure as shown in Figure 2.1a. In this example, the closed surface is represented by metal plate extending to infinity. By selecting the closed surface to correspond with the surface of a metal plate the tangential electric fields are known to be zero over most of the plate (except in the aperture). The original problem is replaced by an equivalent problem by removing the metal plane, and assigning the equivalent electric and magnetic surface currents to the aperture and the metal areas. (See Figure 1.1b) The equivalent magnetic current density M_s in the aperture is given by equation 2.1. The magnetic current density elsewhere will be zero, since the tangential electric field along the metal surface will be zero.

$$M_s = -\hat{n} \times E_t \quad (2.1)$$

Now an imaginary flat electrical conductor is placed over the surface and shorts out the electric current density everywhere. The magnetic current density M_s exists only in the area previously

occupied by the aperture, and it radiates in the presence of the conductor. (See Figure 2.1c.) By image theory, the conductor can be removed and replaced by an imaginary (equivalent) source M_s , as shown in Figure 2.1d. Finally, this equivalent problem reduces to the problem shown in Figure 2.1e (that is the magnetic current density is doubled), and standard formulas can be used to find the radiated fields from the equivalent sources.

This approximation approach is appropriate for applications where the tangential fields are well defined [16][17][18][19][20][21], as in this wave guide example. However, EMI/EMC applications seldom have well behaved fields, such as plane waves. Finding the fields in the aperture with a true EMI source in close proximity to the aperture (non-far field source) is a difficult problem unless numerical techniques are used. (See Chapter 4.)

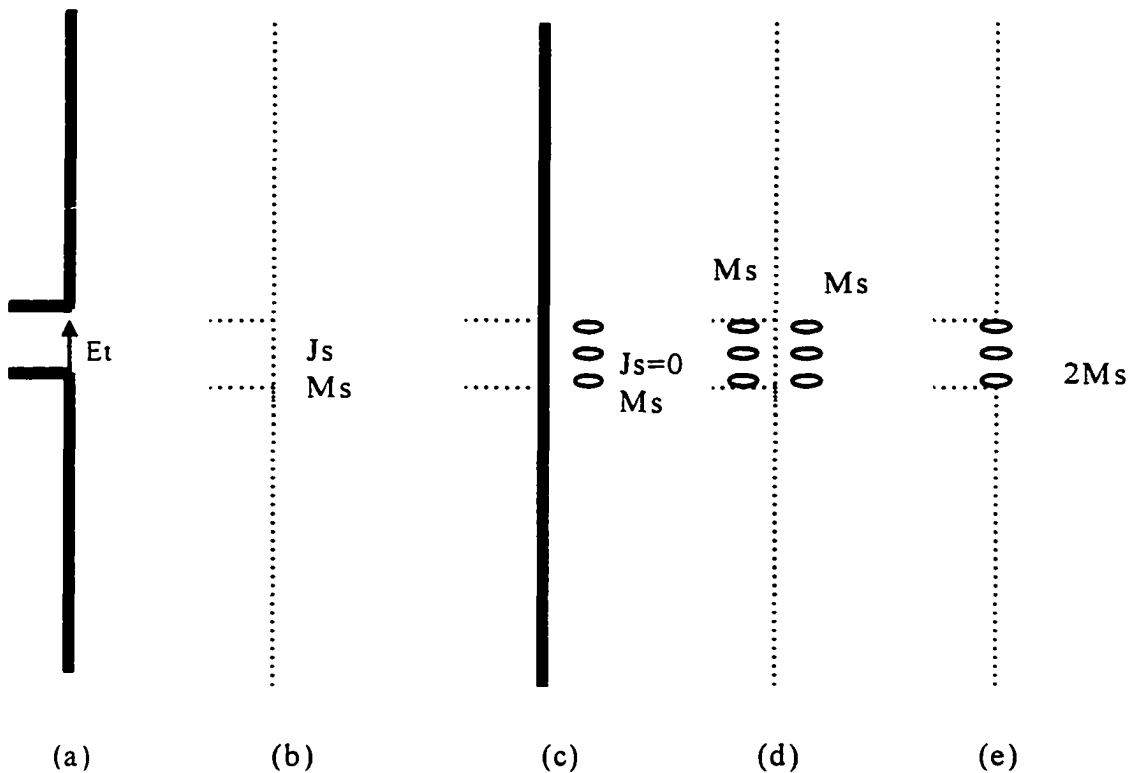


Figure 2. 1 Equivalent Models for Aperture in Infinite Plate

2.3 Closed Form Approaches

There are examples in the literature [15] describing the effect of apertures using closed-form expressions. These efforts all make the assumption that the fields entering the aperture are plane waves. Although these solutions can be used for many electromagnetic applications, they are not particularly useful for EMI problems.

2.4 Summary

Emissions through an aperture in a shielded enclosure, due to sources within the enclosure, can be found once the fields in the aperture are known. Finding the fields within the aperture is difficult in EMI/EMC applications since the source geometry within the enclosure is complex and electrically close to the aperture. The next chapter describes how the FDTD modeling approach can be used to determine the fields in the aperture due to sources within the enclosure.

CHAPTER 3

INTRODUCTION TO THE FINITE-DIFFERENCE TIME-DOMAIN TECHNIQUE

3.1 Background

The Finite-Difference Time-Domain (FDTD) technique is a direct solution method for Maxwell's time-dependent curl equations. FDTD is straightforward to implement on a computer, and possibly more importantly, it is simple to understand and use, while being extremely powerful. It was originally introduced by Kane Yee in 1966 [22] but was not widely used until after 1975 when Taflov published the first validated FDTD models of sinusoidal electromagnetic wave penetration into a three-dimensional metal cavity [23]. Since 1986, FDTD has been extensively used for a wide range of applications involving electromagnetics.

3.2 The Basics of FDTD

As stated above, FDTD is based directly on Maxwell's curl equations (3.1).

$$\begin{aligned}\nabla \times H &= J + \frac{\partial D}{\partial t} \\ \nabla \times E &= -\frac{\partial B}{\partial t}\end{aligned}\tag{3.1}$$

Although the FDTD equations are fully capable of handling materials with volume dielectric displacement currents (J in 3.1), the application of interest in this work is either free space or perfect electrical conductor (PEC). Therefore, since there is no dielectric material and this J term will be always zero in these materials, it is removed to make the explanation of FDTD clearer.

3.2.1 One-dimensional FDTD

The three dimensional Maxwell's equations can be converted to a one-dimensional case to introduce FDTD in (3.2). Simply stated, the spatial change in magnetic field at a point in space is equal to the change in the electric flux density with time; and the spatial change in electric field at a

$$\begin{aligned}\frac{dH}{dx} &= \frac{dD}{dt} \\ \frac{dE}{dx} &= \frac{dB}{dt}\end{aligned}\quad (3.2)$$

point in space is equal to the change in the magnetic flux density with time (ignoring the permittivity and permeability for a moment). Converting these differential equations into central-difference equations (3.3)(3.4), creates a simple set of linear equations. When the terms are rearranged,

$$\frac{H_i^n - H_{i-1}^n}{\Delta x} = \varepsilon \frac{E_i^{n-1} - E_i^n}{\Delta t} \quad (3.3)$$

$$\frac{E_i^n - E_{i-1}^n}{\Delta x} = \mu \frac{H_i^{n-1} - H_i^n}{\Delta t} \quad (3.4)$$

where: i denotes position in space

n denotes time

the equations now provide a solution to the 'new' value of the electric field, based upon the 'old' value of the electric field at that same point, and the difference of the magnetic fields on either side of it (3.5). The 'new' value of the magnetic field, based upon the 'old' value of the magnetic field at that same point, and the difference of the electric fields on either side of it (3.6).

$$E_i^{n-1} = E_i^n + \frac{\Delta t}{\Delta x \varepsilon} (H_i^n - H_{i-1}^n) \quad (3.5)$$

$$H_i^{n-1} = H_i^n + \frac{\Delta t}{\Delta x \mu} (E_i^n - E_{i-1}^n) \quad (3.6)$$

In order to maintain accuracy when converting from differential equations to central difference equations, the spatial position where the central difference is taken is the center between the alternate positions. Figure 3.1 shows the alternating positions of the electric and magnetic fields in space. The distances between adjacent electric or magnetic field points must be small, that is, the

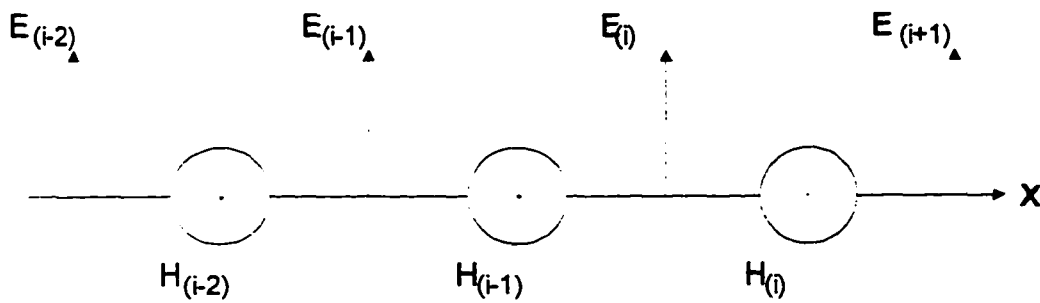


Figure 3- 1 One Dimensional FDTD Grid

fields must not vary rapidly between adjacent points. A normal rule-of-thumb is to require the FDTD grid size to be no larger than 1/10th of the shortest wavelength. For cases where extreme accuracy is required, grid sizes of 1/20th the shortest wavelength are typically used. Since the electric and magnetic fields are not found at exactly the same point, the time when they are calculated must be slightly different as well. Typically, the time calculation for the electric fields is specified at +/- 1/2 time increment. So equations (3.5) and (3.6) become:

$$E_i^{n-1/2} = E_i^{n-1/2} + \frac{\Delta t}{\Delta x \epsilon} (H_i^n - H_{i-1}^n) \quad (3.7)$$

$$H_i^{n-1} = H_i^n + \frac{\Delta t}{\Delta x \mu} (E_i^{n-1/2} - E_{i-1}^{n-1/2}) \quad (3.8)$$

3.2.2 Two-dimensional FDTD

When the above formulation is expanded into two dimensions, there will be three fields to solve. for example: either E_x , E_y , and H_z or H_x , H_y , and E_z . A typical two dimensional FDTD grid is shown for the TM case in Figure 3.2. (Although the TM case is shown here, the TE case can also be used.) Note the same basic conditions apply, that is, the 'new' value of the magnetic field (H_z , where 'z' is out of the page) is dependent on the 'old' magnetic field at that point, and the difference between the E_x components on either side of it, and the difference between the E_y components on either side of it.

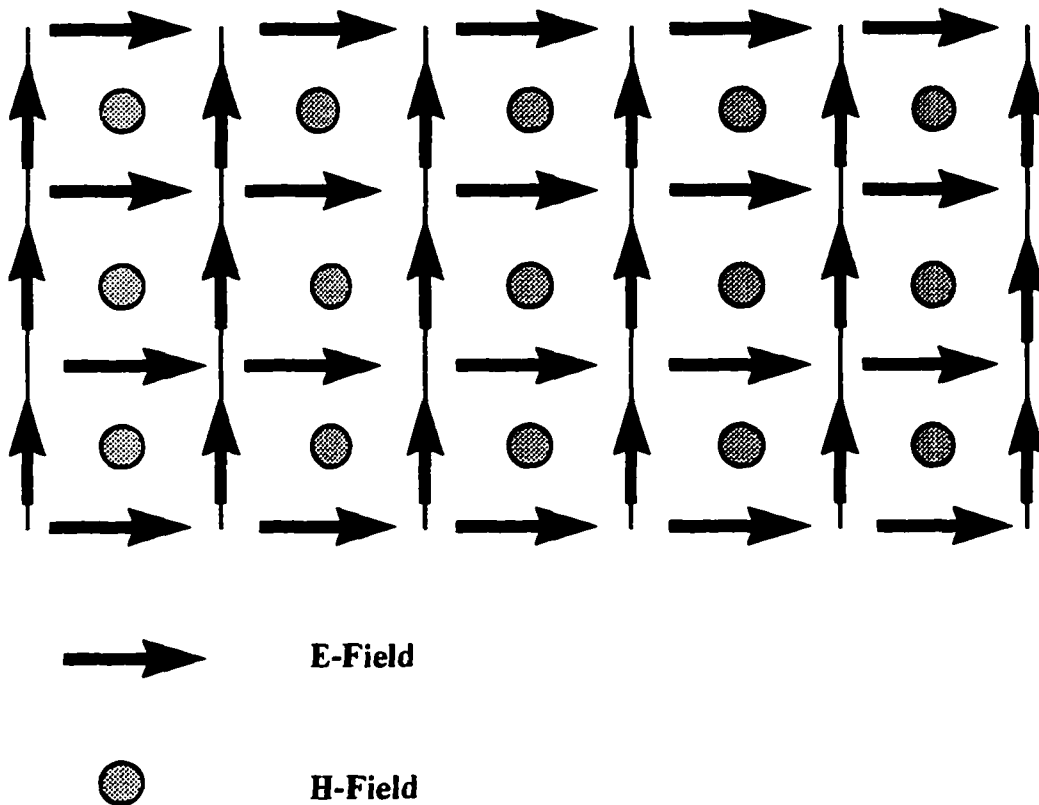


Figure 3- 2 Two Dimensional FDTD Grid

As before, the 'new' value of the electric field is found from the 'old' value of electric field at that point, and the difference between the magnetic fields on either side of it. The FDTD two-

dimensional equations are given in (3.9), (3.10) and (3.11) for this case, but the opposite case with E_z , H_x , and H_y can easily be found as well.

$$E_{x(t,j)}^{n-1/2} = E_{x(t,j)}^{n-1/2} + \frac{\Delta t}{\Delta x \epsilon} (H_{z(t,j)}^n - H_{z(t,j-1)}^n) \quad (3.9)$$

$$E_{y(t,j)}^{n-1/2} = E_{y(t,j)}^{n-1/2} + \frac{\Delta t}{\Delta y \epsilon} (H_{z(t,j)}^n - H_{z(t-1,j)}^n) \quad (3.10)$$

$$H_{z(t,j)}^{n-1} = H_{z(t,j)}^n + \frac{\Delta t}{\Delta y \mu} (E_{x(t,j)}^{n-1/2} - E_{x(t,j-1)}^{n-1/2}) - \frac{\Delta t}{\Delta x \mu} (E_{y(t,j)}^{n-1/2} - E_{y(t-1,j)}^{n-1/2}) \quad (3.11)$$

3.2.3 Three Dimensional FDTD

The above FDTD expressions can be expanded into full three dimensions (as used in this effort). Although difficult to draw many 3-D cells, a single cell is shown in Figure 3-3. The three electric fields are found along the axis, while the magnetic fields are found in the center of the face of the cube. Although the example in Figure 3-3 is a cube, the shape of the FDTD cell can be any rectangular shape. Typically, the aspect ratio of the 3-D FDTD cell is kept to 3:1 or less.

The basic operation of FDTD remains the same as earlier, that is, the 'new' electric field E_x is found from the 'old' electric field E_x , and the difference between adjacent H_z fields and the difference between adjacent H_y fields. Similar descriptions apply for the other five fields. Equations (3.12) through (3.17) show the simplified three dimensional FDTD equations.

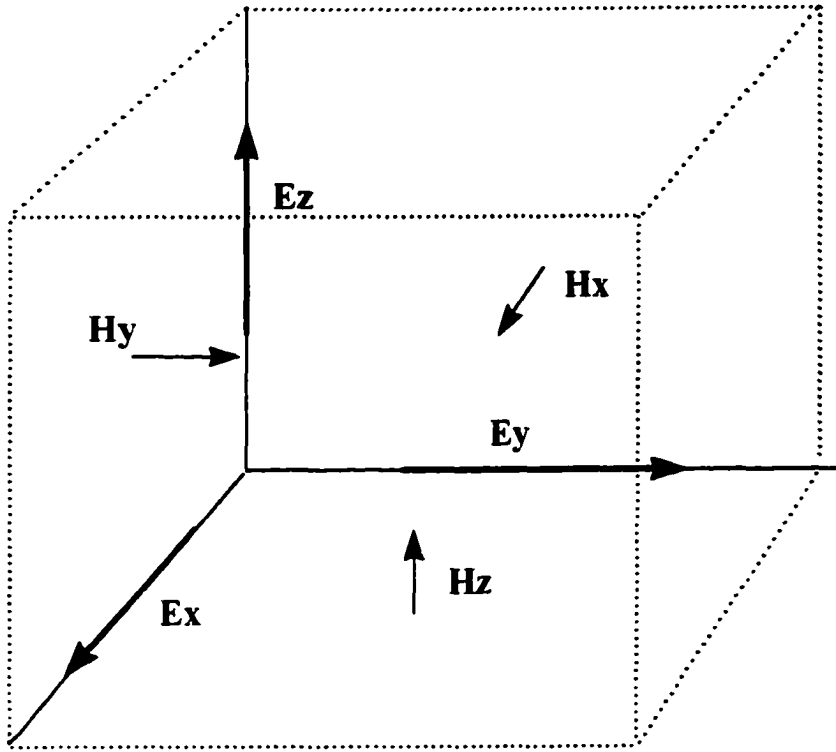


Figure 3- 3 Three Dimensional FDTD Cell

$$H_{x(i,j,k)}^{n-1/2} = H_{x(i,j,k)}^n + \frac{\Delta t}{\Delta z \mu} (E_{y(i,j,k)}^{n-1/2} - E_{y(i,j,k-1)}^{n-1/2}) - \frac{\Delta t}{\Delta y \mu} (E_{z(i,j,k)}^{n-1/2} - E_{z(i,j-1,k)}^{n-1/2}) \quad (3.12)$$

$$H_{y(i,j,k)}^{n-1/2} = H_{y(i,j,k)}^n + \frac{\Delta t}{\Delta x \mu} (E_{z(i,j,k)}^{n-1/2} - E_{z(i-1,j,k)}^{n-1/2}) - \frac{\Delta t}{\Delta z \mu} (E_{x(i,j,k)}^{n-1/2} - E_{x(i,j,k-1)}^{n-1/2}) \quad (3.13)$$

$$H_{z(i,j,k)}^{n-1/2} = H_{z(i,j,k)}^n + \frac{\Delta t}{\Delta y \mu} (E_{x(i,j,k)}^{n-1/2} - E_{x(i,j-1,k)}^{n-1/2}) - \frac{\Delta t}{\Delta x \mu} (E_{y(i,j,k)}^{n-1/2} - E_{y(i-1,j,k)}^{n-1/2}) \quad (3.14)$$

$$E_{x(i,j,k)}^{n-1/2} = E_{x(i,j,k)}^{n-1/2} + \frac{\Delta t}{\Delta y \epsilon} (H_{z(i,j,k)}^n - H_{z(i,j-1,k)}^n) - \frac{\Delta t}{\Delta z \epsilon} (H_{y(i,j,k)}^n - H_{y(i,j,k-1)}^n) \quad (3.15)$$

$$E_{y(i,j,k)}^{n-1/2} = E_{y(i,j,k)}^{n-1/2} + \frac{\Delta t}{\Delta z \epsilon} (H_{x(i,j,k)}^n - H_{x(i,j,k-1)}^n) - \frac{\Delta t}{\Delta x \epsilon} (H_{z(i,j,k)}^n - H_{z(i-1,j,k)}^n) \quad (3.16)$$

$$E_{z(i,j,k)}^{n-1/2} = E_{z(i,j,k)}^{n-1/2} + \frac{\Delta t}{\Delta x \epsilon} (H_{y(i,j,k)}^n - H_{y(i-1,j,k)}^n) - \frac{\Delta t}{\Delta y \epsilon} (H_{x(i,j,k)}^n - H_{x(i,j-1,k)}^n) \quad (3.17)$$

3.3 Stability Conditions

The size of the FDTD cell must be set to be electrically small (small compared to the shortest wavelength) to satisfy the linearity assumption when converting from the derivative to central-difference equations. However, the size of the time step must also be small to ensure stability.

The limit of the size of the time steps is given by the Courant Stability Condition [27] in equation (3.18).

$$\Delta t \leq \frac{1}{c \sqrt{\frac{1}{\Delta x^2} + \frac{1}{\Delta y^2} + \frac{1}{\Delta z^2}}} \quad (3.18)$$

Since equation (3.18) uses c (the speed of light) it sets the maximum time step for free space. For applications where the speed of propagation is less than c (for example in a dielectric), then the slowest propagation velocity must be used instead of c in (3.18).

3.4 Absorbing Radiation Boundary Conditions

One important use of FDTD is in geometries with 'open' regions where the spatial domain of the computed field is unbounded in one or more coordinate directions. Clearly, no computer can store an unlimited amount of data, and so the computational domain must be limited in size. Although the computational domain must be large enough to enclose all the physical features of the model, it must be small enough to allow reasonable calculation times.

Since there is a limit to the size of the computational domain, there must be some boundary condition to ensure there is no non-physical (and unwanted) artificial reflection from the edge of the

computational domain. As is seen in Figure 3.1 and equations 3.5 and 3.6, the 'new' electric field value at any point is found by using the 'old' electric field values, and the difference between the magnetic fields *on either side of that point*. However, at the edge of the computational domain there is no magnetic field outside the electric field on the boundary, and some other means to find this outer electric field is needed. It is not correct to simply set fields outside the computational domain to zero, since this would effectively place a perfect electrical or magnetic conductor along the boundary (depending upon which field is set to zero). Therefore, an absorbing boundary condition (ABC) is needed to simulate free space to approaching fields to ensure they do not reflect from the edge of the computational domain.

The simplest ABC would be to force the far-field relationship in (3.19) and find the outer electric fields

$$E = 120\pi H \quad (3.19)$$

from the magnetic fields and the wave impedance of free space. This is not practical, since the knowledge of the magnetic fields is not known at the point where the electric field is needed. Some other means to find the outer value of the electric field is needed.

Quite a number of different ABC's have been proposed in the literature. Some are better than others, that is, less error (apparent artificial reflection), and some take more processing resources than others. The most popular ABC's in use today are the Mur [24], Higdon [25], and Liao [26] ABC's. Comparisons between these and others can be found in the references [27][28], and are not be repeated here. All these ABC's operate correctly when the approaching fields are 'far-

fields', that is, the relationship between E and H is as shown in equation 3.19. The amount of error (unwanted reflection) increases dramatically when the far-field condition is not maintained.¹ This results in so-called 'white space' around the model elements of interest to ensure the far-field condition is met. The white space is typically $1/6^{\text{th}}$ lambda at the longest wavelength of interest (since this distance is commonly used as the distance where the far-field condition exists between the E and H fields). This results in much larger computational domain (to include the necessary white space) than is required for simply the model itself.

3.5 Summary

The FDTD technique is a fairly simple and straightforward technique, but very powerful nevertheless. FDTD solve Maxwell's curl equations by converting them to central difference equations, and solving the electric field and magnetic fields in leap-frog fashion.

The above description is intended to provide a general review of the FDTD technique. The reader is encouraged to use [27] and [28] for further reading of the FDTD technique.

¹ All ABC's require the far-field relationship between the electric field and the magnetic field except the recently developed ABC's by Ramahi [29][30] and Berenger [31].

CHAPTER 4

STAGE ONE MODEL USING FDTD

4.1 Introduction

As stated in the introduction, the first stage of the hybrid model is to estimate the fields in the aperture of an enclosure using FDTD. The second, and final, stage of the hybrid approach is to use the fields found in the first stage as the excitation source for an MoM model to enable the modeling of fields outside of the enclosure. In order for the hybrid approach to be valid, the aperture field distribution modeled by FDTD in stage one must be the same as the field distribution modeled by MoM in stage two. The objective of this chapter is to present FDTD modeled data showing field behavior in an aperture and its sensitivity to source geometry and frequency. A similar study of MoM-modeled fields in an aperture, presented in Chapter 7, shows that the field distribution for both techniques is nearly identical.

4.2 Characterizing Aperture Field Distribution using FDTD

FDTD has been shown to correctly model radiation through an aperture in earlier studies (e.g., [23] and [32]), although little attention has been paid to the fields within the aperture. Further, earlier work did not investigate sources in very close proximity to the aperture, a condition that will exist in many EMC scenarios, nor did they investigate cases where the electrical distance between the aperture and absorbing boundary becomes small at low frequencies.

To characterize the distribution of the electric field in the aperture and the effects of different source-to-aperture configurations, the aperture impedance is used here to determine sensitivity to the effects of angle of illumination, source distance, and distance from the aperture to the absorbing boundary. The effect that is observed, as detailed below, is that for frequencies below the first resonance of the aperture, field distribution is nearly invariant to source location, which makes implementation of the hybrid approach straightforward, as is shown in Chapter 8.

As a rule of thumb, apertures are normally constrained to be shorter than a half wavelength at the internal clock frequencies and harmonics of the clock frequency. This means this effort can focus on the emission leakage of apertures at frequencies below the first resonance frequency of the aperture. For example, a clock frequency of 100 MHz with a rise time of 5 ns will typically include significant harmonic energy up to the 12th harmonic (1200 MHz). The corresponding maximum aperture size would be 125 mm for this maximum harmonic frequency.

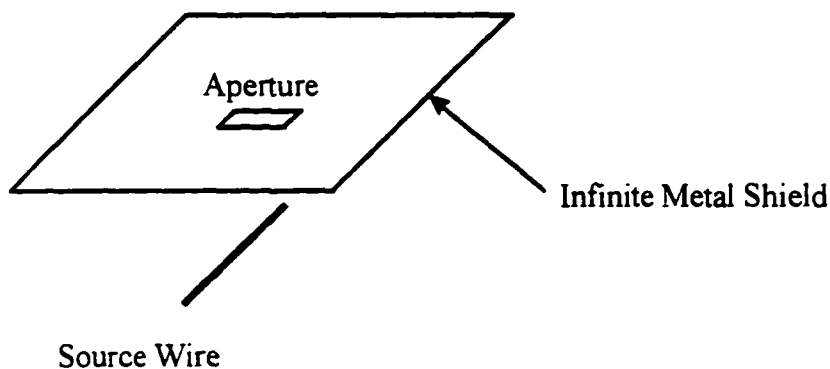


Figure 4. 1 Single Aperture in Infinite Conducting Sheet

4.3 Aperture Impedance

The impedance of a particular location within the aperture is frequency dependent and is found by dividing the electric field by the magnetic field at the same point in space. The FDTD technique was used to model the aperture in the infinite metal plate by extending the metal plate to ABC. A diagram of the FDTD computational space used for single-aperture modeling is shown in Figure 4.2.

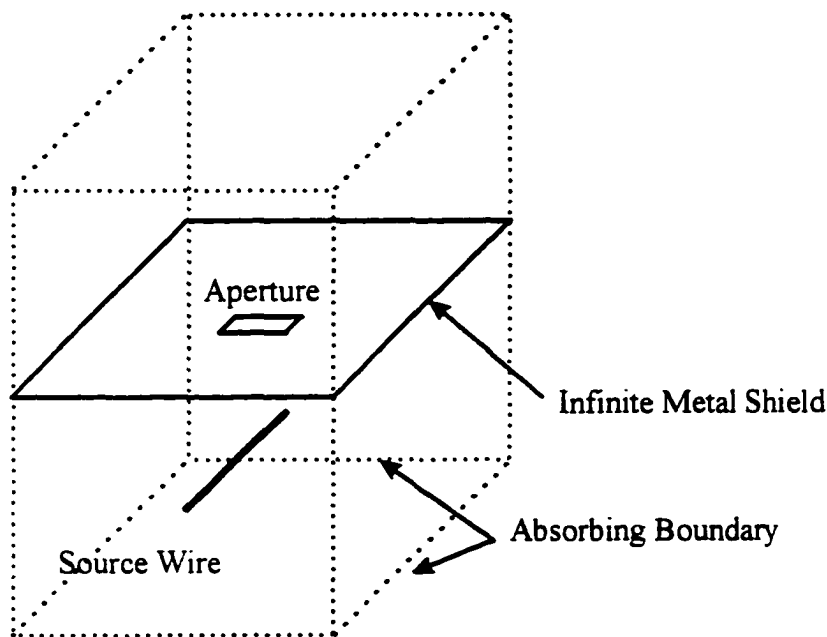


Figure 4. 2 FDTD Model for Single Aperture in Infinite Metal Sheet

It is recognized that the inherent offset between the electric and magnetic fields in FDTD will have an effect on the calculation of impedance, however earlier work has shown that this $\frac{1}{2}$ cell offset will result in only negligible error [33]. Hence, that offset will be ignored here.

Because there are two orthogonal pairs of electric and magnetic fields in the aperture, there are two possible aperture impedances as defined by the equations below:

$$Z_{xy} = \frac{E_x}{H_y} \quad (4.1)$$

$$Z_{yx} = \frac{E_y}{H_x} \quad (4.1a)$$

Figure 4.3 shows a typical modeled impedance vs. frequency curve for a point within an aperture. The impedance is very low at frequencies well below resonance, and increases to a maximum at the lowest resonant frequency. This is consistent with expectations, since the aperture can be considered a high impedance source (electric-field source), with little or no field transmission at

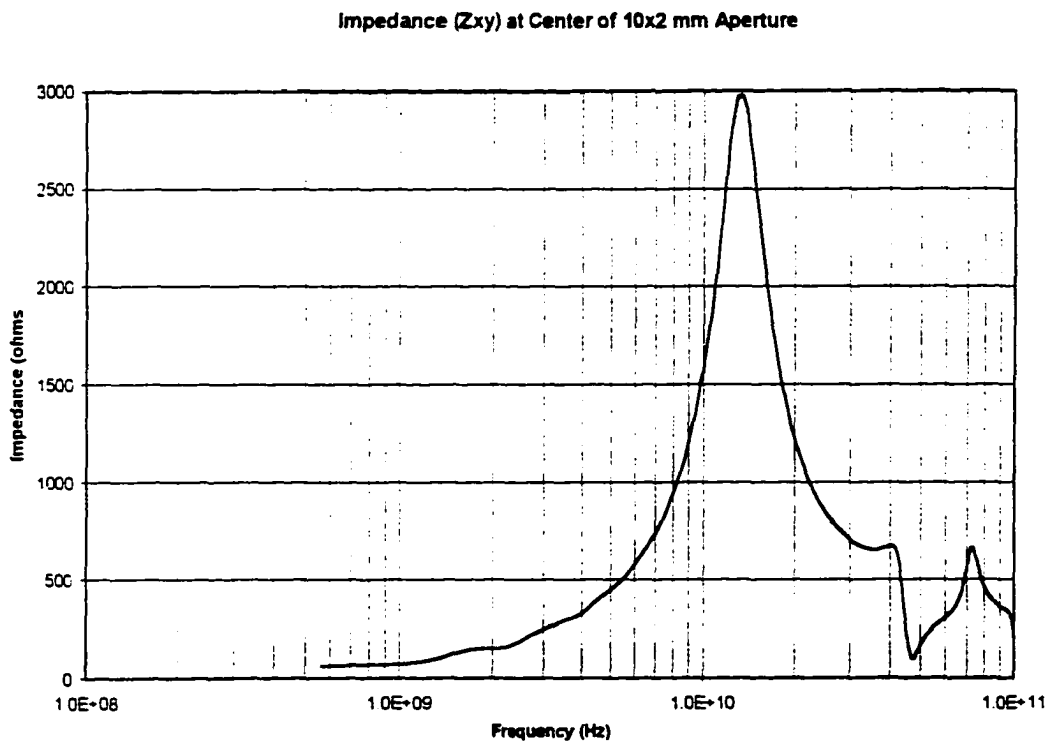


Figure 4. 3 Typical Aperture Impedance vs. Frequency

low frequencies. As the frequency increases, the field transmission increases to a maximum at the frequency where the aperture length is 1/2 wavelength. While the impedance is very low over the low frequency region, the aperture acts like a conductor, and shorts out a significant portion of the

tangential electric field. When the impedance is high the electric field is no longer shorted, and the electric field level in that area will increase accordingly. This electric field across the aperture is seen from the outside of the aperture, and is therefore transmitted to the outside environment. As the impedance is sampled within the aperture, it will vary depending upon the observation position within the aperture. The family of curves in Figure 4.4 show the impedance along the center line of the aperture for one half of the aperture. (The field distribution, and therefore the impedance, is symmetrical in the aperture.) The electric field levels within the aperture are seen to be a maximum in the center of the aperture (at frequencies below the first resonant frequency), and taper to zero at the ends of the aperture, similar to the impedance.¹ The magnetic fields tend to vary very little across the aperture.

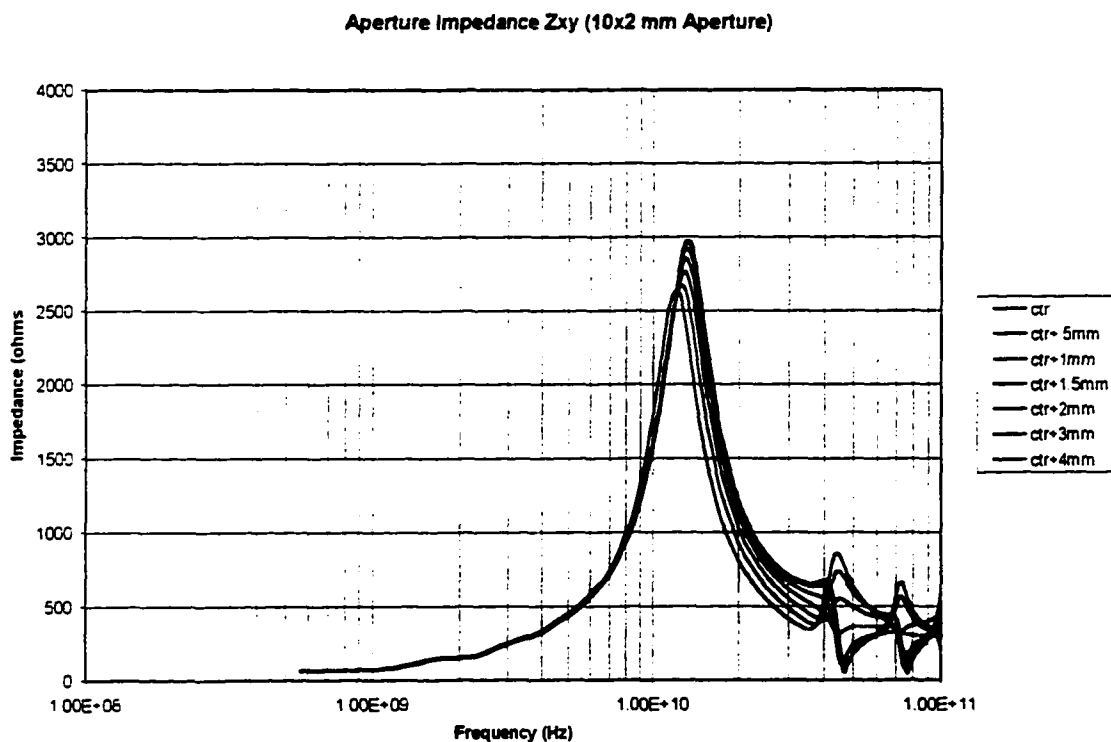


Figure 4. 4 Typical Aperture Impedance Along Aperture

¹ Z_{xy} is used as this example since it is the dominant impedance. Z_{yx} is discussed briefly in a later section.

4.4 Single Aperture Model

The goal of this section is to determine the distance between the aperture and the ABC necessary to achieve good results inside the aperture, and to demonstrate the impedance in the aperture does not significantly change when the source distance or source illumination angle is varied.

4.4.1 Computational Domain Size

Figure 4.5 shows the three dimensional FDTD computational space and the various sizes of computational domain used to find the fields within the aperture. The size of the initial aperture was 10 mm x 2 mm. The FDTD cell size was 0.5 mm, which resulted in an aperture of 20 x 4 cells.

As can be seen in Figure 4.6, the impedance for a 10 x 2 mm aperture is affected by the amount of white space² above the aperture. At the frequency of the first resonance (15 GHz) the wavelength is 20 mm, so the far field (using the 1/6 lambda rule) begins at a distance of only 3+ mm. Since each cell is 0.5 mm (in this case), the 50 cell white space is much more than is needed at 15 GHz. However, since the frequencies below resonance are also important, the required white space must be extended to about 55 mm at 1 GHz (110 cells), and further at lower frequencies. As can be seen in Figure 4.6, the impedance is very low at low frequencies in this example, and so the impact of the absorbing boundary condition is not apparent.

² White space is the commonly used term for the extra FDTD space outside the true model which is required to provide the distance between any radiating source and the absorbing boundary condition along the computational domain's edge.

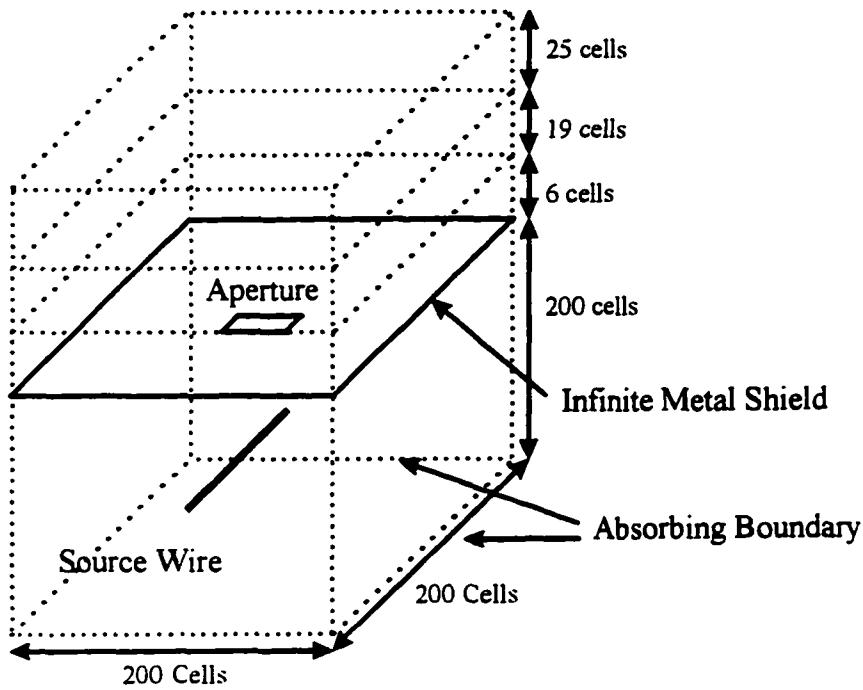


**Figure 4. 5 FDTD Model for Single Aperture
with Different Computational Domain Sizes**

A larger aperture (20 x 2 mm) was modeled to determine the effect of aperture distance to the ABC. Figure 4.7 shows that more effect was observed at the lower frequencies, since more of the energy at those frequencies is present with the larger aperture. From these various tests, it was decided to use at least 50 white space cells above the aperture to find the impedance in the aperture.

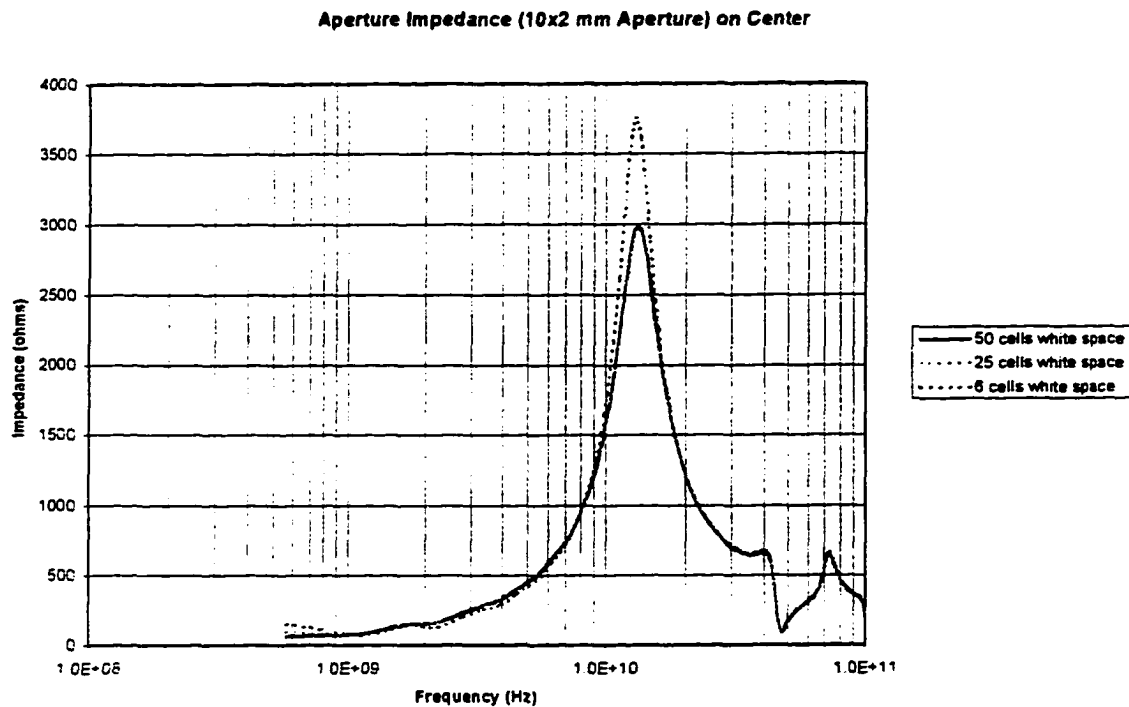


**Figure 4. 6 Impedance Variation in Aperture Center
Due to White Space Above Aperture (10x2 mm Aperture)**

4.4.2 Aperture Resonant Frequency

As stated earlier, the resonant frequency is apparent from the impedance curves. Resonance is expected at the frequency where the length of the slot is $1/2$ wavelength (using Babinet's principle [34]). For a slot 10 mm long, the first resonant frequency is expected at 15 GHz, which corresponds to the highest impedance in Figure 4.8. Upon closer examination of the frequency where the highest impedance occurs, it is not at 15 GHz, but at 13.5 GHz. This is due to the fact that the aperture has a thickness (1 mm), which acts similar to an extension plate or disk on the end of a dipole antenna, lowering the resonant frequency. Figure 4.8 and Appendix A Figures A-1

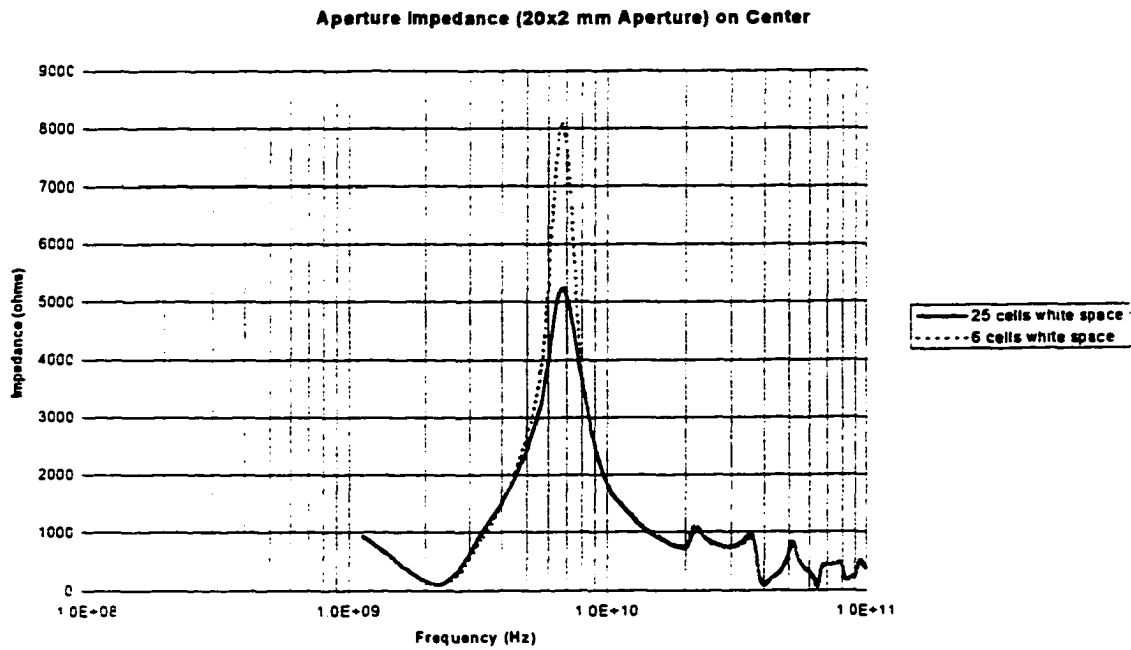


**Figure 4. 7 Aperture Impedance Variation
Due to White Space for 20x2 mm Aperture**

through A-4 give examples of the FDTD modeled impedance at the center of the aperture for different sized apertures. The effect of resonant frequency vs. aperture length is shown in Figure 4.9.

4.4.3 Source Position and Illumination Angle

To study the effect of source position on aperture impedance a number of different source positions were investigated, allowing the angle of illumination to vary over a range of 90 degrees (perpendicular or straight on) to 26 degrees. The impedance in the center of the aperture is shown for the various angles of illumination in Figure 4.10. As can be seen in this figure, the impedance

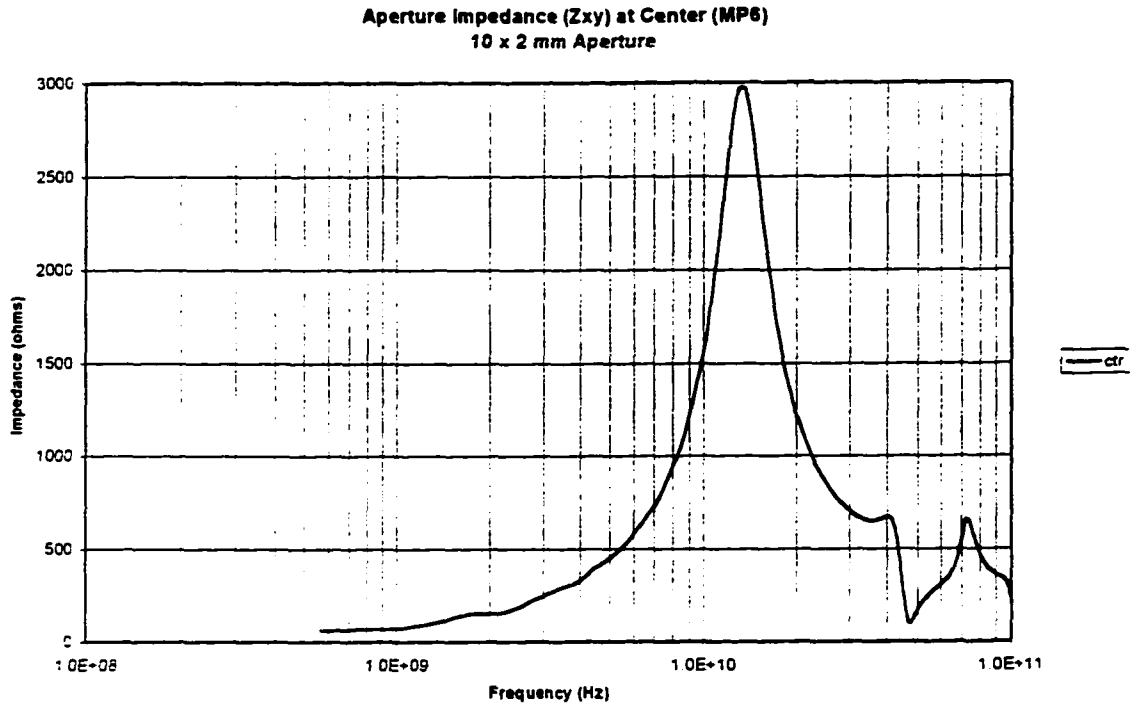


Figure 4. 8 Z_{xy} Impedance at Center of 10x2 mm Aperture

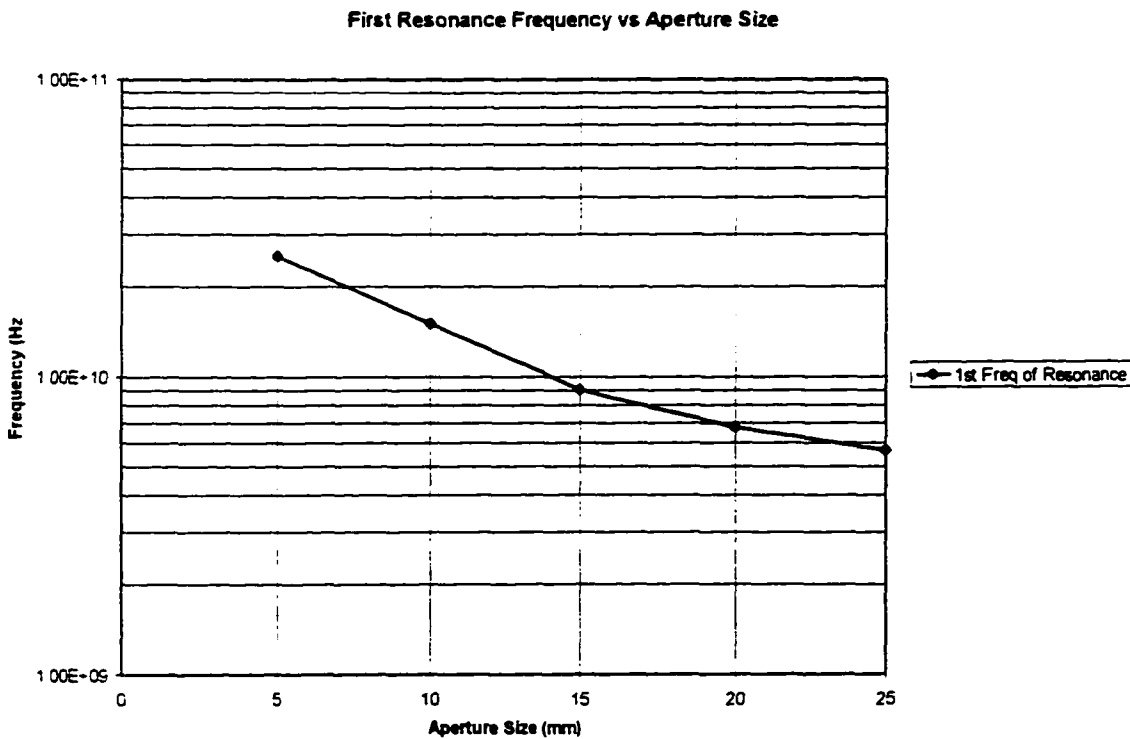


Figure 4. 9 Aperture First Resonant Frequency for Different Size Apertures

is nearly independent of the source position from low frequencies to well above the first resonance. Once the second resonant frequency is reached the impedance varies dramatically (with respect to frequency). However, this does not impact this effort, since the apertures are constrained to be smaller than a half wavelength long at the first resonant frequency. Therefore, the aperture impedance is independent of illumination angle over the frequency range of interest.

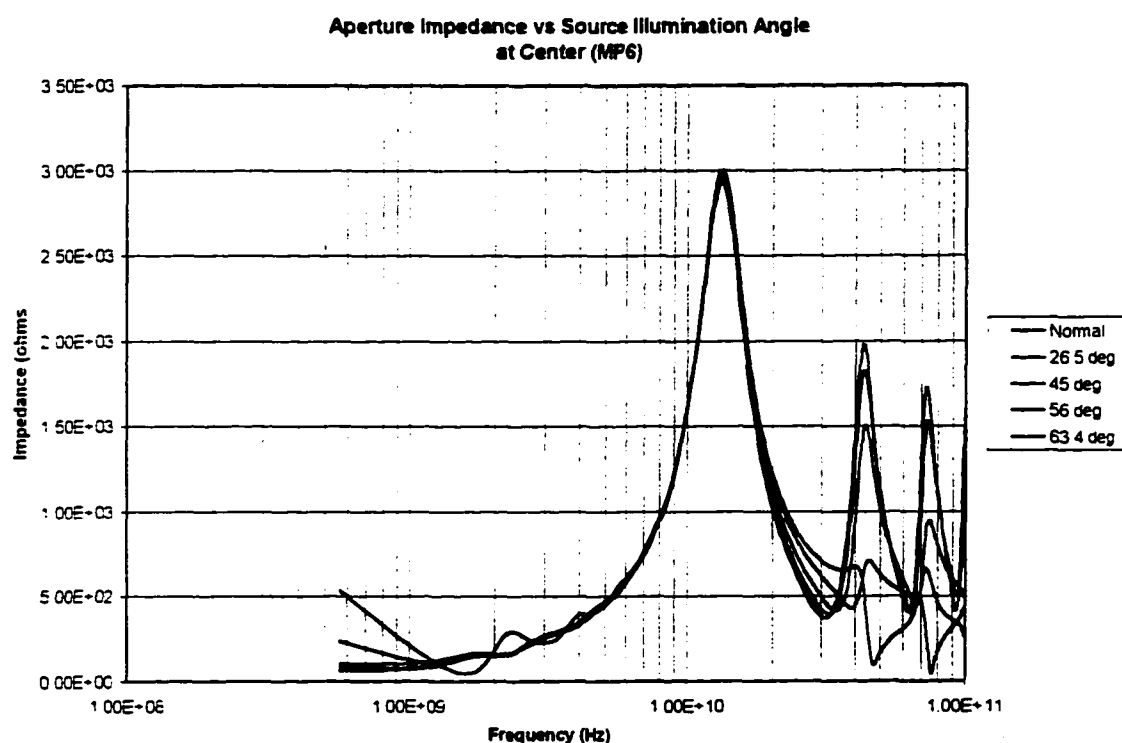
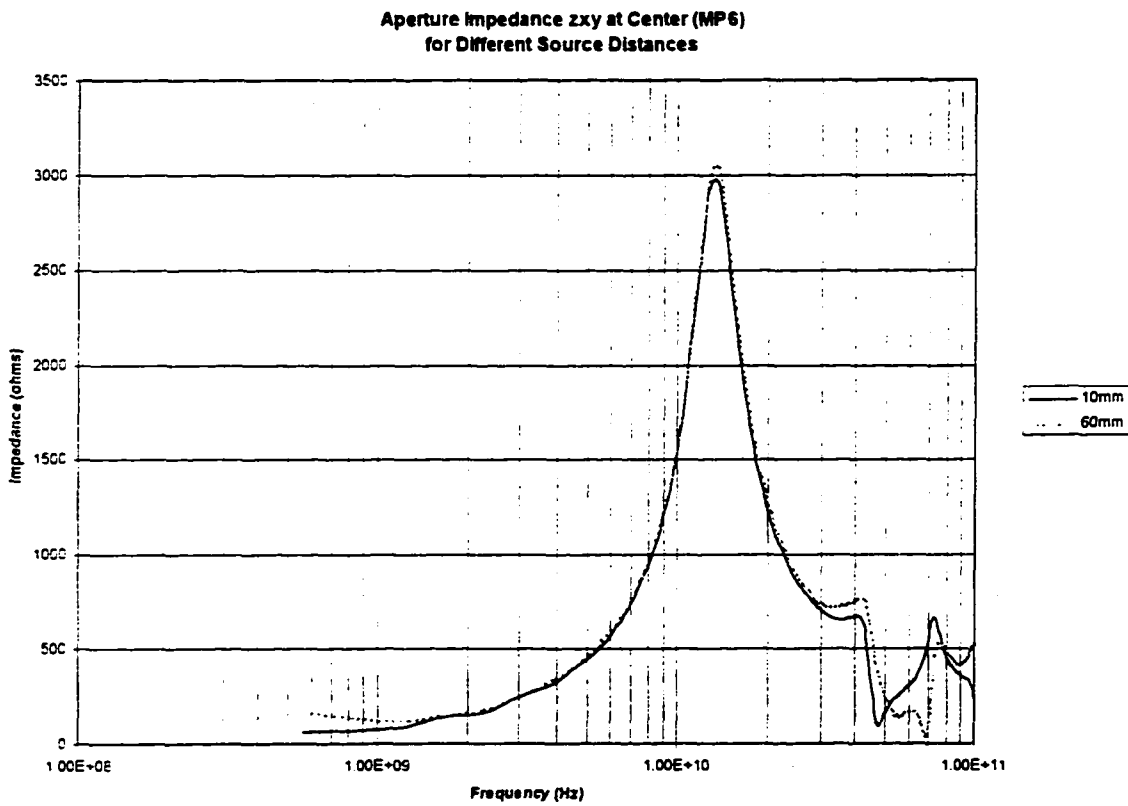


Figure 4. 10 Aperture Impedance Due to Source Illumination Angle (10x2 mm)

4.4.4 Source distance from Aperture

In the previous sections, the distance between the source wire and the aperture was typically 20 cells (10 mm). This close proximity between the source and the aperture will likely occur when modeling practical configurations, and it can introduce errors at low frequencies. Fortunately, these errors can be compensated, as is shown in Chapter 5.

The effect on the impedance in the aperture was examined as the source distance was increased to 120 cells (60 mm). This puts the aperture in the far field of the source above 833 MHz. As can be seen in Figure 4.11, there is no discernible difference in the impedance in the center of the aperture for the different source positions. Naturally, the electric and magnetic field levels do vary with source distance, but the relationship between the electric and magnetic fields (i.e. impedance) does not vary. Therefore, the aperture impedance can be considered to be independent of the distance between the source and the aperture for this study.



**Figure 4.11 Effect of Source Distance on Aperture Impedance Z_{xy}
for 10x2 mm Aperture (ctr)**

4.4.5 Impedance Variation Along the Aperture

The impedance along the aperture varies with position. It is maximum in the center of the aperture, and decreased as the observation point approaches the edge of the aperture for frequencies below resonance. The Z_{xy} impedance is defined as the perpendicular polarized impedance (where the electric field is perpendicular to the aperture's longest dimension). The Z_{yx} impedance is defined as the parallel polarized impedance (where the electric field is parallel to the aperture's longest dimension).

Three different sized apertures were examined. The sizes were 10 mm by 2 mm, 20 mm by 2 mm, and 5 mm by 2 mm. The amplitude of the impedance was found to vary as a function of position, but the shape of the impedance as a function of frequency remained the nearly same as at the aperture center (shown in Figure 4.8 and Appendix A Figures A-1 through A-4). As expected, the impedance decreases as the observation point moves closer to the edge of the aperture, since this aperture edge will tend to force the tangential electric field zero.

Figures 4.12 and Appendix A Figures A-6 through A-7 show the variation of the impedance with position for selected frequencies. The frequencies were selected to include below first resonance, at first resonance, and above first resonance frequencies. In general, the variation of the impedance with position was sinusoidally shaped. (Some anomalies were seen and is discussed in a later section.) This sinusoidal shape was expected, since it fits well with the current distribution on a dipole antenna. The impedance must go to zero at the edge of the aperture (PEC walls), and will be at maximum at the center of the aperture (below resonance). The amplitude of the maximum impedance (at resonance) for the various aperture sizes is shown in Figure 4.13.

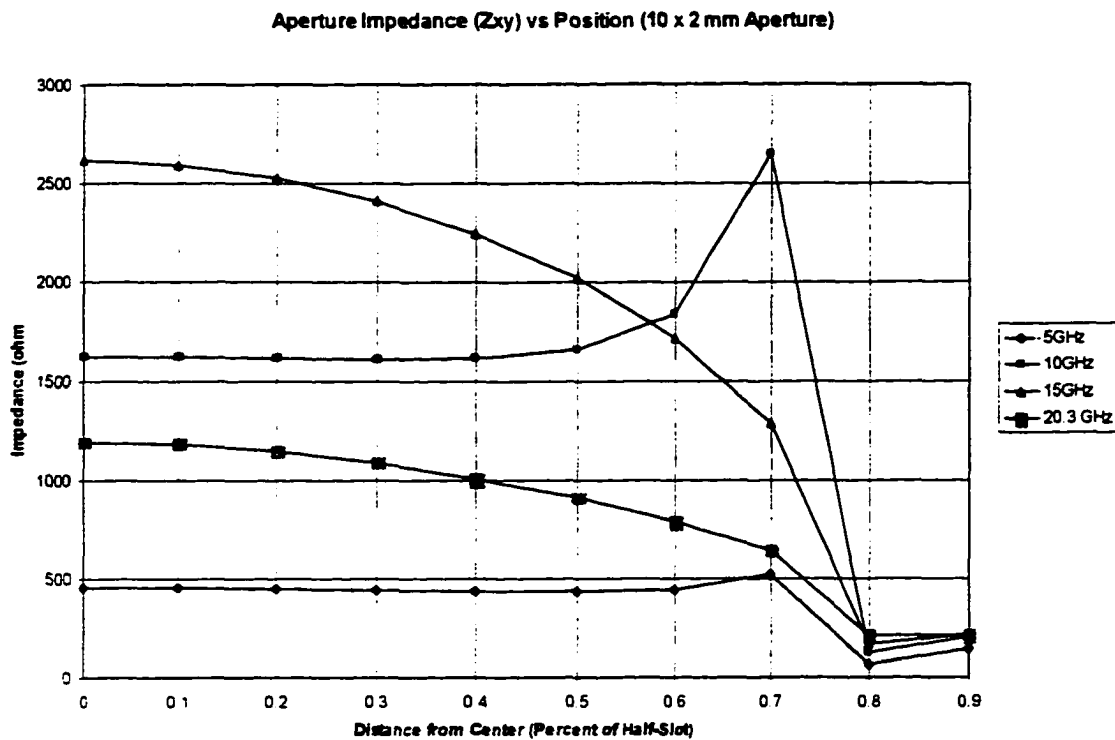


Figure 4.12 Variation of Impedance (Z_{xy}) Along Aperture (10x2 mm)

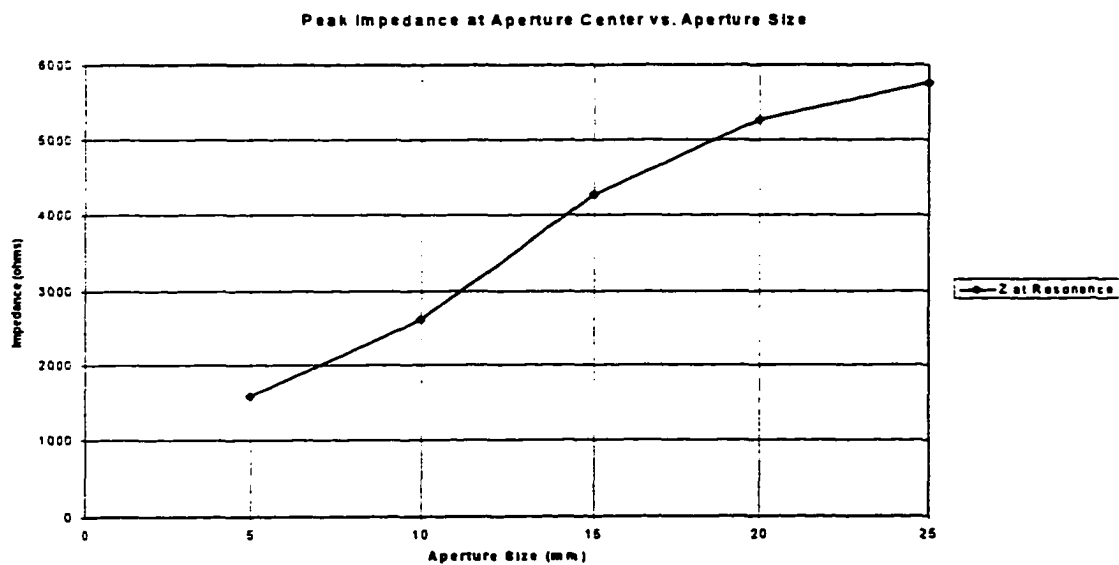


Figure 4.13 Maximum Impedance Z_{xy} (at First Resonant Frequency) for Various Aperture Sizes

Parallel-Polarized Impedance

All the previous impedance values were for Z_{xy} , that is, for the impedance where the electric field is perpendicular to the aperture's major dimension. This is the polarization where the greatest amount of emission leakage will occur.

The parallel-polarized impedance varies only slightly across the aperture, and is at least 40-60 dB less than the Z_{xy} impedance levels. Since the Z_{yx} impedance is very low compared to the Z_{xy} impedance throughout the frequency range of interest, the E_y electric field will also be very low. The EMI measurement process typically provides a measurement accuracy of +/- 3 dB. Since a high degree of modeling accuracy is not generally required for EMI/EMC applications, the aperture can be modeled with no electric field polarized in the y-direction, and hence only the x-polarized electric field is used to characterize the fields in the aperture in the approach addressed here.

4.4.6 FDTD Impedance Anomalies

At low frequencies, the impedance is expected to vary similar to a Herizian dipole in agreement with Babinet's principle. However, at low frequencies the modeled impedance did not always agree with the expected impedance. This results from the fact that the electrical distance between the aperture and the ABC begins to encroach upon the $1/6^{\text{th}}$ wavelength limit at the lower frequencies. Chapter 5 shows a method to compensate for the errors introduced by the ABC at low frequencies

4.5 Multiple Apertures

Most practical problems include multiple apertures. These multiple apertures can be of the form of an air cooling vent area, a series of option slots in the rear of a personal computer, or for other

applications. Consequently, the modeled effects of an additional, side-by-side aperture are documented here which show that the second aperture does not introduce unexpected errors.

In the configuration modeled here, the apertures were both cross polarized with the source, and were separated along their length by 2 mm (equal to their width). Both apertures were 10 mm long. Figure 4.14 shows a drawing of the dual aperture configuration. Figure 4.15 shows the impedance for different points across one of the apertures. The family of curves are very similar to the single aperture cases. Figure 4.17 shows the variation of the impedance across the aperture, which is very similar to the results in Figure 4.12 for the single aperture case.

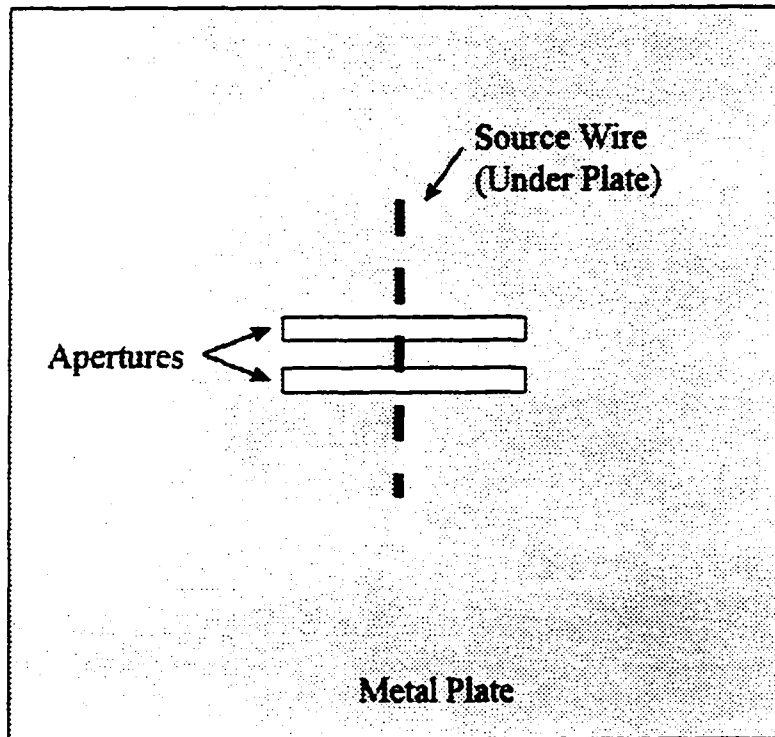
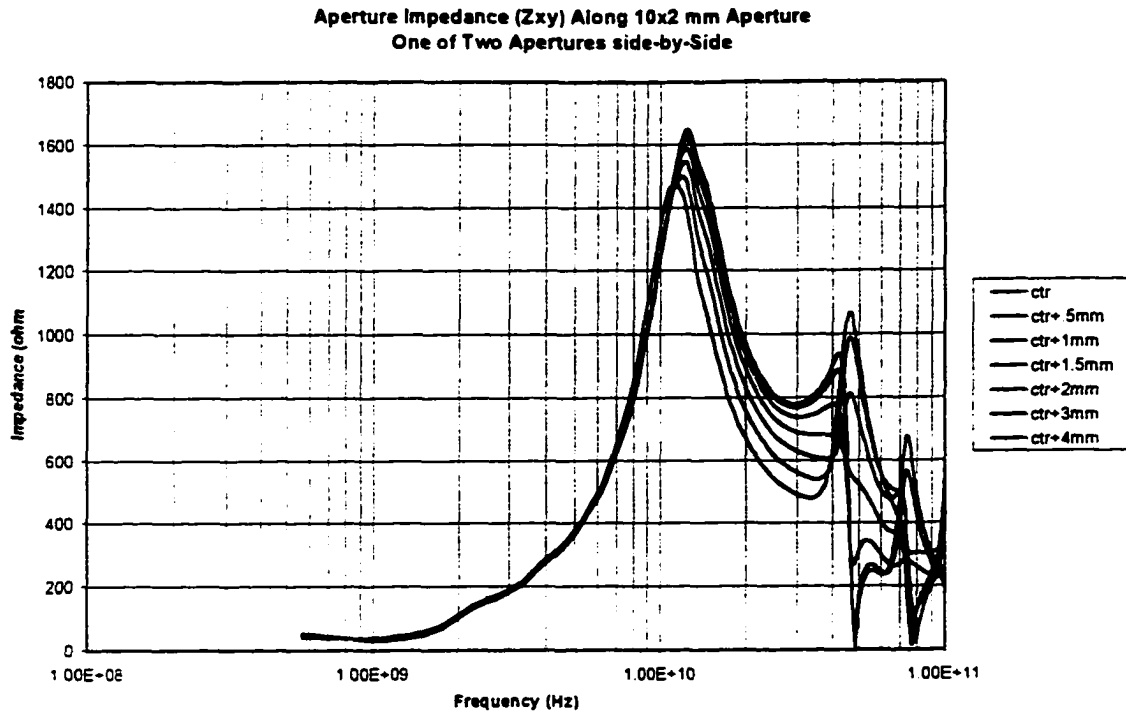
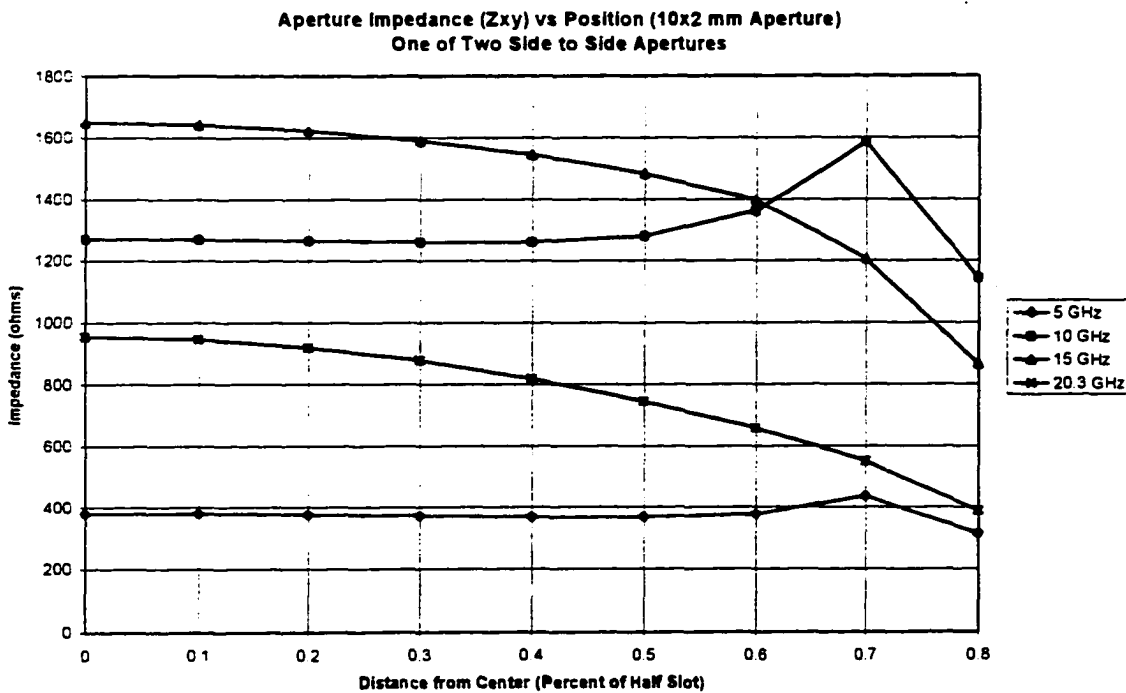


Figure 4. 14 Dual Aperture Configuration



**Figure 4. 15 Impedance (Z_{xy}) Along Aperture (10x2 mm)
(One of Dual Configuration)**



**Figure 4. 16 Variation of Impedance (Z_{xy}) Along Aperture (10x2 mm)
(One of Dual Configuration)**

4.6 Summary

This chapter shows that the impedance within the aperture varies in a predictable manner over the frequencies of interest. Importantly, the impedance distribution below resonance is independent of the source position, source illumination angle, and number of apertures. Consequently, the fields within the aperture can be represented by the field at the center of the aperture, regardless of how the source/components are arranged within the enclosure containing the aperture. This can result in a significant simplification in implementing the hybrid approach, since only the field components at the center of the aperture, rather than for the entire aperture, will need to be stored. This simplification is valid only if the MoM-modeled fields in an aperture, excited by a source at its center, are the same as those estimated by FDTD. Chapter 7 addresses the modeling of apertures using FDTD and MoM, and documents that the field distributions are nearly identical for both techniques.

At low frequencies where the impedance curves do not vary according to theory or expectation, some form of compensation must be used to determine the correct field values. That compensation technique is the subject of the next chapter.

CHAPTER 5

CORRECTING THE ELECTRIC FIELDS WITHIN THE APERTURE AT LOW FREQUENCIES

5.1 Introduction

Chapter 4 showed how to find the fields in an aperture using FDTD, as long as the frequency was sufficiently high to insure the absorbing boundary conditions (ABC) constraints were not violated. However, at low frequencies where the ABC is not functioning properly due to the lack of sufficient distance between the computational boundary and the aperture (the effective source), the aperture impedance and therefore the electric field levels are not correct. Since these aperture fields will be used by the second stage of the hybrid technique (in Chapter 7) as the source of the fields outside the shielded enclosure, this error introduced by the ABC must be compensated for or the final results of the hybrid technique will also be incorrect.¹

¹ For example, using the $1/6^{\text{th}}$ lambda rule, if the edge of the aperture is only 35 cells from the ABC, and the cells are .5 mm on a side, then the errors could be expected for frequencies below 3 GHz. Depending upon the fundamental clock frequency, EMI engineers must be concerned with frequencies as low as 30 MHz, and so this correction is important to most EMI engineering applications.

There are three possible techniques available to correct the aperture field values at low frequencies: (1) increase the computational domain size in the original FDTD model to allow sufficient white space around the aperture to eliminate the errors at low frequencies, (2) use the Surface Impedance Boundary Condition (SIBC) with an FDTD model, and (3) use a Herzian dipole impedance technique to find the correct aperture impedance and electric field values. Unfortunately, it is not always practical to increase the computational domain sufficiently to allow the ABC to be far enough away to operate correctly at frequencies with wavelengths in the range of 3 to 10 meters, since the amount of FDTD cells, and the corresponding required computer RAM, would be excessive. For example, to correctly operate at 50 MHz, the ABC must be 1 meter minimum in all directions from the ABC. Using the same ½ mm cells size as earlier (to allow FDTD to correctly describe the aperture), the ABC must be at least 2000 cells away from the aperture in all directions. This would require at least 64 billion cells.

The SIBC allows the use of the true aperture impedance without requiring a large external white space to find the fields within the aperture. However, this requires a FDTD model to be run to first find the aperture impedance. This aperture impedance must then be corrected at low frequencies using the Herzian dipole impedance method, and then the FDTD model run again with the SIBC. So unless the aperture impedance is known in advance (through a previous modeling effort), the SIBC is computationally very expensive.

The Herzian dipole impedance technique has the advantage that it is quite easy to implement, and allows the user to find both the corrected aperture impedance and the corrected aperture electric fields quickly. Once this corrected electric field is found, it can then be used in the second stage of the hybrid technique as the source for the external fields.

5.2 Using Herzian Dipole Impedance Technique to Correct the Low Frequency Aperture Impedance

Since the aperture impedance at low frequencies found using the stage one FDTD models is incorrect due to errors introduced by the too-close proximity of the ABCs, an Herzian dipole impedance method is used to correct these impedances. This correction can be omitted when the FDTD model results are in error at frequencies outside the range of to the specific project. However, if the low frequencies are of interest, (as in most EMI activities) the field levels must be corrected or errors will result in the final results.

Close examination of the aperture impedance curves showed that at frequencies above where the ABC's error was introduced, the impedance varies according to expectation. Experiments with larger FDTD computational domains, and thus greater distances between the ABC and the aperture, shows this region to extend to lower frequencies.

In the case of a long, thin aperture, Babinet's principle [34] allows the aperture to be represented by an equivalent sized linear antenna. Since aperture impedance is incorrect at frequencies where the wavelength is long compared to the aperture size, the equivalent dipole antenna will be electrically short. The radiation impedance for a short, Herzian dipole is given in equation (5.3). The radiation impedance from the Herzian dipole can be normalized and used to predict the correct impedance in the aperture at low frequencies.

$$Z_{Pred} = 80\pi^2 \left(\frac{l}{\lambda} \right)^2 \quad (5.3)$$

where: l is the length of the Herzian dipole

As can be seen in Figure 5.1, the original FDTD impedance at these lower frequencies has been corrected.

The original impedance at low frequencies was fairly well behaved in the case of the 10 x 2 mm aperture. The correction of the impedance at low frequencies is more important in cases where the low frequency impedance is not well behaved. Figure 5.2 shows the impedance found in Chapter 4 for a longer aperture (20 x 2 mm), and the effects of the FDTD ABC is clear at the lower frequencies.

The impedance at low frequencies (below 4 GHz) is again found using the normalized Herzian dipole radiation impedance. The corrected and original impedances are shown in Figure 5.3.

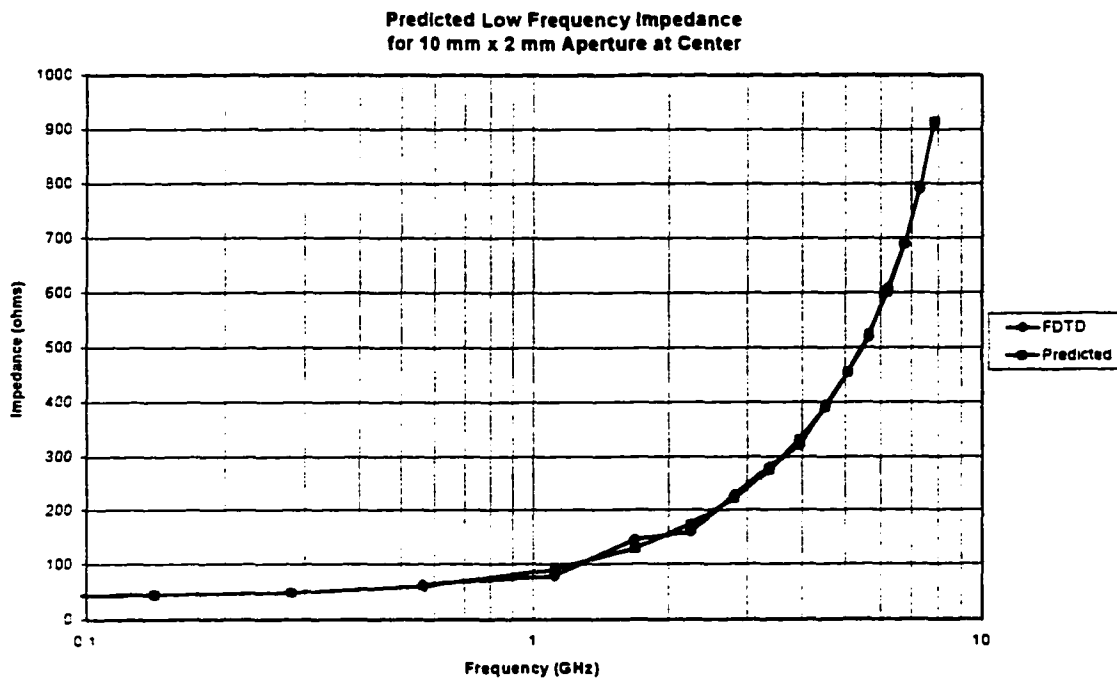


Figure 5. 1 Comparison of Extrapolated and FDTD-original Aperture Impedance

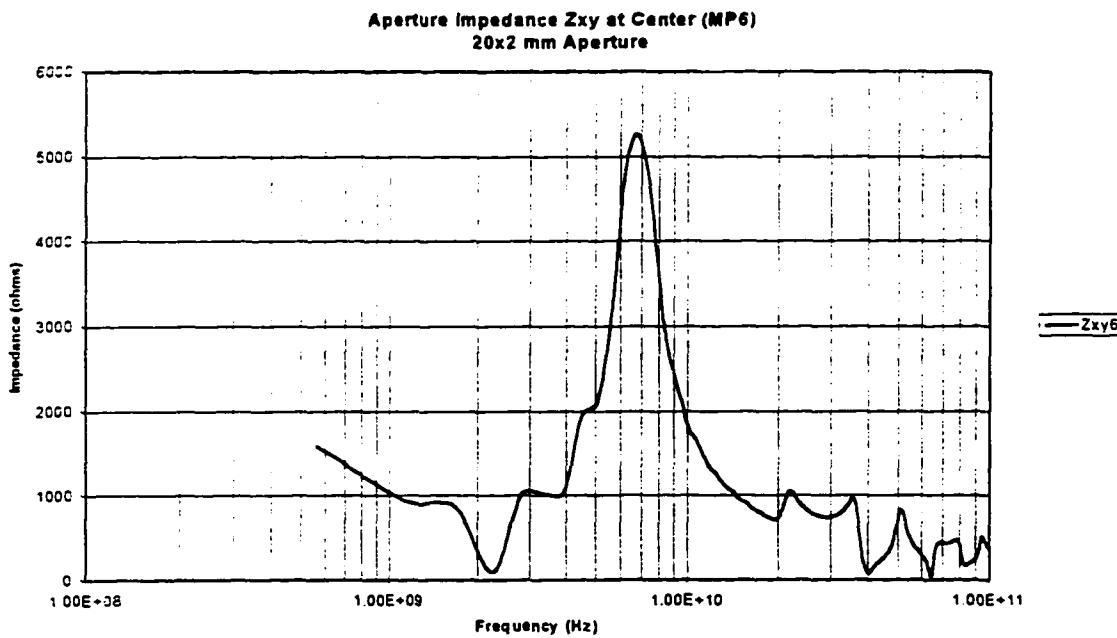
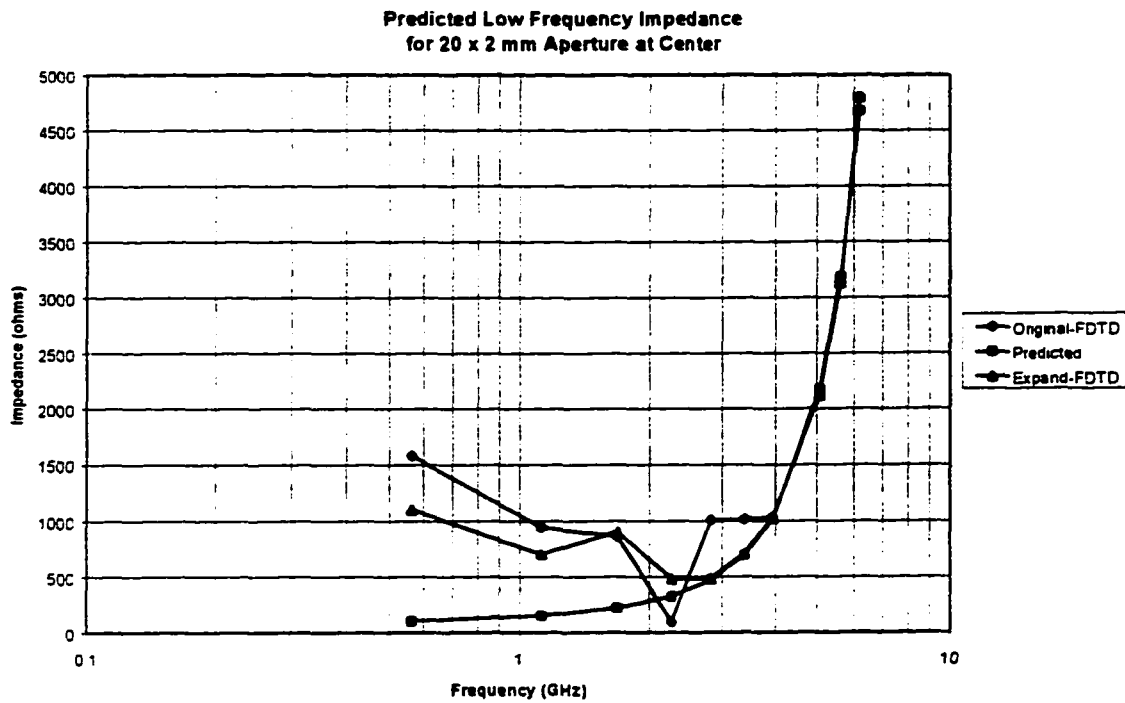


Figure 5. 2 Original Impedance for 20x2 mm Aperture



**Figure 5.3 Original FDTD and Corrected Aperture Impedance
for 20x2 mm Aperture**

The computational domain size can be increased to observe the effect on the impedance at lower frequencies and insure equation 5.3 correctly predicted this impedance. Figure 5.3 shows the impedance in the center of the aperture when the FDTD computational domain is expanded to double the original size. Although this expanded computational domain is impractical this FDTD model maintains the previous good agreement and extends the good agreement to lower frequencies (before the ABC's again corrupt the impedance).

5.3 Correcting the Electric Fields in the Aperture at Low Frequencies

The previous sections show how to use the Herzian dipole impedance to correct the impedance at low frequencies. However, the real goal is to find the correct electric field levels in the aperture for use in the second stage of the hybrid technique. The electric field levels are directly proportional to the impedance. Since the impedance at low frequencies is found using the expected Herzian dipole impedance the corrected values of the electric field at low frequencies can be found using the same curve normalized to the electric field values.

Figure 5.4 shows an example of the corrected electric field at low frequencies using the Herzian dipole technique. This figure shows the results for the 20 x 2 mm aperture (this aperture size had a more dramatic electric field error at low frequencies than most of the other sizes). The fields from this technique agree with the original FDTD electric field levels at frequencies where the ABC was not contributing an error, and provide the correct electric field strengths at the lower frequencies.

5.4 Summary

This chapter briefly discusses the different possible techniques to correct the impedance and electric field levels in the aperture, and then demonstrates how a technique based upon Babinet's principle and Herzian dipole radiation impedance is sufficient to correct these quantities at low frequencies. The corrected low frequency electric field levels are now used as the final output of the Stage One, and as the input (or source) in Stage Two of the hybrid technique.

The corrected low frequency aperture impedance could also be used for SIBC implementation within a second FDTD model. However, this approach is computationally expensive and time consuming unless the aperture impedance is to be used in a number of different FDTD models.

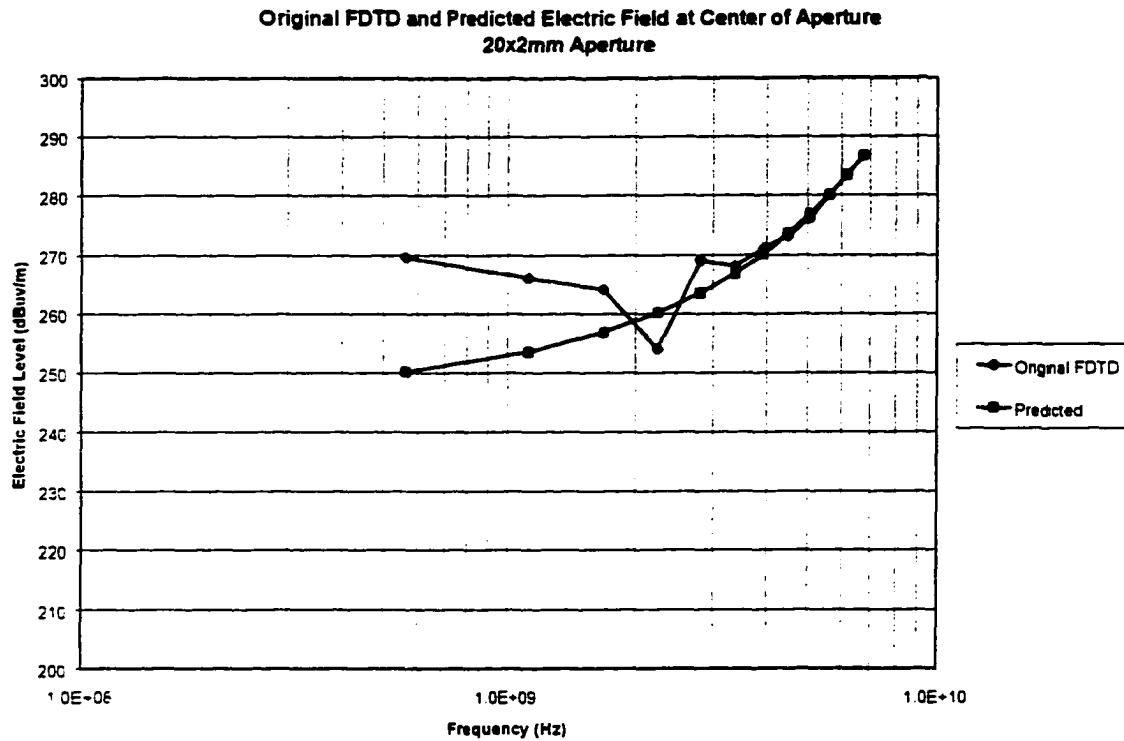


Figure 5. 4 Original FDTD and Corrected Electric Field Level in Aperture

CHAPTER 6

INTRODUCTION TO THE METHOD OF MOMENTS TECHNIQUE

6.1 Background

This chapter provides a brief introduction to the Method of Moments technique. This technique is used in the Stage Two part of the hybrid modeling technique. Readers already familiar with MoM may wish to skip straight to Chapter 7.

The Method of Moments technique (also called Moment-method technique) have become very popular in the past 30 years or so. MoM algorithms are generally run on high speed workstation or mainframe computers, but they can be used to model a wide variety of problems without requiring the user to assume a particular current distribution. MoM is used extensively to model radar cross section and antenna applications, and has recently been applied to EMI/EMC problems.

The structure to be modeled is converted into a series of metal plates and wires. In fact, often a solid structure is converted into a wire frame model, eliminating the metal plates. Once the structure is defined, the wires are broken into wire segments (short compared to a wavelength so the assumption of constant current on that segment is valid) and the plates are divided into patches

(small compared to a wavelength so the assumption of constant current on that patch is valid).

From this structure, a set of linear equations is created. The solution to this set of linear equations is the RF currents on each wire segment and surface patch. Once the RF current is known for each segment and patch, the electric field at any point in space can be determined by solving for each segment/patch and performing the vector summation.

6.2 The Basics of MoM

MoM actually refers to a general procedure for solving linear mathematical equations of the form.

$$L(\vec{f}) = \vec{E} \quad (6.1)$$

where L is a linear operator f is an unknown response and E is a known excitation. [35][36][37]

For electromagnetic modeling, the known excitation is usually an imposed electric or magnetic field, and the unknown response is generally a current distribution. Once the currents are known everywhere on the structure, the electric and magnetic fields can be found at any point in space.

The equation relating the currents and fields is known as the electric field integral equation (EFIE) when the known excitation is an electric field or the magnetic field integral equation (MFIE) when the excitation is a magnetic field. The relative usefulness and accuracy of a particular MoM model depends, in part, on the assumptions made in the process of deriving the integral equation and whether EFIE or MFIE is used. For EMI/EMC modeling, the source is usually an applied voltage (modeled as an electric field across a short distance), so the EFIE is typically used.

The first step in the MoM solution process is to describe the unknown response (in this case the current distribution) as a finite sum of basis functions,

$$\vec{f} = \sum_{j=1}^N \alpha_j \vec{f}_j \quad (6.2)$$

where: \vec{f}_j = the j^{th} basis function

α_j = unknown coefficient

Using this approximation the entire current distribution can now be solved by finding the values for the N coefficients, α_j

The second step in the MoM procedure is to define a set of weighting functions, w_i , which may or may not be the same as the basis functions. Defining the inner product as,

$$\langle A, B \rangle \equiv \oint_s (A \cdot B) ds \quad (6.3)$$

where s is the entire surface on which A and B are defined. We can then take the inner product of (6.1) with each of the chosen weighting functions,

$$\langle \vec{w}_i, L(\vec{f}) \rangle = \langle \vec{w}_i, \vec{E} \rangle \quad i = 1, 2, \dots, N \quad (6.4)$$

Using the linearity of L and making the substitution in equation (6.2),

$$\sum_{j=1}^N \alpha_j \langle \vec{w}_i, L(\vec{f}_j) \rangle = \langle \vec{w}_i, \vec{E} \rangle \quad (6.5)$$

Setting:

$$\bar{Z}_j = \langle \bar{w}_j, L(\bar{f}_j) \rangle$$

$$\bar{I}_j = \alpha_j$$

$$\bar{E}_j = \langle \bar{w}_j, \bar{E} \rangle$$

And converting to matrix notation:

$$[\bar{Z}][\bar{I}] = [\bar{E}] \quad (6.6)$$

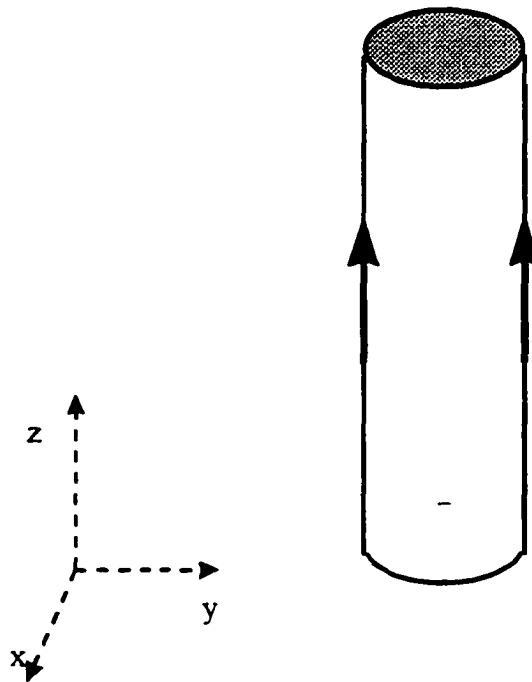


Figure 6. 1 MoM Geometry for Current on a Wire Segment

The only unknown quantity in equation (6.6) is \mathbf{I} , which is a vector containing the N coefficients describing the current distribution. Provided the matrix \mathbf{Z} is not singular (that is, the problem has a unique solution), it is possible to solve for \mathbf{I} in equation (6.6) as shown in equation (6.7).

$$[\bar{I}] = [\bar{Z}]^{-1}[\bar{E}] \quad (6.7)$$

Therefore, the current on a particular segment in the model is found from the contribution of the source, and the contribution from all other currents in the model. Equation (6.7) represents a set of N linear equations, with N unknowns.

6.3 Filling the Impedance Matrix

Once the basics of MoM are understood, the next task is to fill the impedance matrix, then the MoM solution simply requires inverting [Z] and a matrix multiplication with the source. Although there are a number of different formulations to find [Z], this work used a thin-wire formulation called Pocklington's integral equation. In general, the electric field from a current is given by

$$\bar{E}(r) = -j\omega \bar{A} - j\frac{1}{\omega\mu\epsilon}\nabla(\nabla\cdot\bar{A}) = -j\frac{1}{\omega\mu\epsilon}(\omega^2\mu\epsilon\bar{A} + \nabla(\nabla\cdot\bar{A})) \quad (6.8)$$

where:

$$\bar{A}(r) = \mu\iint_s \bar{J}_s(r')\frac{e^{-j\beta R}}{4\pi R}ds' \quad (6.9)$$

However, since the observation of the current is only along the surface, and only the z component is needed (see Figure 6.1) equation (6.8) is re-written as:

$$E_z(r) = -j\frac{1}{\omega\mu\epsilon}\left(\beta^2 A_z + \frac{\partial^2 A_z}{\partial z^2}\right) \quad (6.10)$$

and with only the z component equation (6.9) becomes:

$$A_z = \frac{\mu}{4\pi} \int_{-l/2}^{l/2} \int_0^{2\pi} J_z \frac{e^{-j\beta R}}{R} a d\phi' dz' \quad (6.11)$$

since the wire is assumed to be thin ($\lambda \gg a$), the current density J_z is not a function of the azimuth angle ϕ , and the current density becomes:

$$J_z = \frac{1}{2\pi a} I_z(z') \quad (6.12)$$

where I_z is assumed to be an equivalent filament line current located on the wire segment's surface.

Therefore,

$$A_z = \frac{\mu}{4\pi} \int_{-l/2}^{l/2} \left[\frac{1}{2\pi a} \int_0^{2\pi} \frac{e^{-j\beta R}}{R} a d\phi' \right] dz' \quad (6.13)$$

$$R = \sqrt{(x-x')^2 + (y-y')^2 + (z-z')^2} \quad (6.13a)$$

$$R = \sqrt{\rho^2 + a^2 - 2\rho a \cos(\phi - \phi') + (z-z')^2}$$

where ρ is the radial distance to the observation point and a is the radius.

Since the wire segment is symmetrical about ϕ , the observation of the current is not a function of ϕ , so $\phi=0$ will be substituted into equation (6.13). Since the observation of the current is on the surface of the wire, $\rho=a$, and equation (6.13) becomes.

$$A_z(\rho = a) = \mu \int_{-l/2}^{l/2} I_z(z') G(z, z') dz' \quad (6.14)$$

$$G(z, z') = \frac{1}{2\pi} \int_0^{2\pi} \frac{e^{-j\beta R}}{4\pi R} d\phi' \quad (6.14a)$$

$$R(\rho = a) = \sqrt{4a^2 \sin^2\left(\frac{\phi'}{2}\right) + (z - z')^2} \quad (6.14b)$$

where equation (6.14a) is a Green's Function. Combining equations (6.10) and (6.14), the electric field is

$$E_z = -\frac{1}{j\omega\epsilon} \int_{-l/2}^{l/2} I(z') \left[\left(\frac{d^2}{dz^2} + \beta^2 \right) G(z, z') \right] dz' \quad (6.15)$$

Equation (6.15) is referred to as Pocklington's integrodifferential equation [38], and it is used to determine the current along the surface of the wire, given an incident electric field.

As mentioned earlier, the selected weighting function varies depending upon the requirements for the modeling. If the segment length is kept electrically small ($1/10^{\text{th}}$ wavelength or shorter), then the point-matching method is commonly used for a weighting function. That is, the current is assumed to only exist on the center of the wire segment as a delta function. Since

$$\int_{-\infty}^{\infty} I_z \cdot \delta(z - z_0) dz = I_z(z = z_0) = I_{z=z_0} \quad (6.16)$$

equation (6.15) can be reduced to

$$E_z = -\frac{1}{j\omega\epsilon} I(z'_{z0}) \int_{-l/2}^{l/2} \left[\left(\frac{d^2}{dz^2} + \beta^2 \right) G(z, z') \right] dz' \quad (6.17)$$

Also, since we assume the wire segment is very thin ($a \ll \lambda$), then equation (6.14a) reduces to

$$G(z, z') = G(R) = \frac{e^{-j\beta R}}{4\pi R} \quad (6.18)$$

Recall in Equation (6.6) the electric field was a function of the unknown current and the impedance. Equation (6.17) fills this function, and the impedance matrix can be created, allowing the currents to be found.

6.4 Finding the Electric Fields from the RF Currents

Once the currents are known, the electric and magnetic fields can be found at any point in space (due to those currents), by using the Herizian dipole equations. The wire segments must be electrically short ($\lambda \gg L$), but this requirement is necessary for the MoM technique and is already implemented. The general electric fields can be found using Equations (6.19) and (6.20).

$$E_r = \frac{IL \cos\theta}{2\pi\epsilon_0} \left(\frac{1}{cr^2} + \frac{1}{j\omega r^3} \right) \quad (6.19)$$

$$E_\theta = \frac{IL \sin\theta}{4\pi\epsilon_0} \left(\frac{j\omega}{c^2 r} + \frac{1}{cr^2} + \frac{1}{j\omega r^3} \right) \quad (6.20)$$

6.4 Summary

The MoM technique is a fairly straightforward and intuitive technique. Creating a wire structure, finding the current distribution over the entire structure, and then finding the fields due to those currents is intuitive to most engineers. The MoM technique requires the creation of a system of N linear equations with N unknowns, where each unknown is the current on a single segment. The unknown currents are solved by using matrix techniques. Once the current is known, the fields can be found using the Herzian dipole equations.

CHAPTER 7

HYBRID TECHNIQUE STAGE TWO MODELING

USING MOM

7.1 Introduction

In this chapter, an effective procedure to predict the fields outside the aperture and shielded enclosure due to an excitation within the enclosure is described. Using the FDTD approach outlined in the previous chapters, the field in the aperture can be accurately and efficiently predicted. Once the aperture field is calculated, it is then used as the driving function for the second stage of modeling, which concerns only the outside region.

The calculations of the aperture impedance (Chapter 4) shows that the aperture impedance and the electric field levels are highest at the center of the aperture, providing the aperture is not electrically large. Therefore, the level of the electric field in the center of the aperture determined in the Stage One model (and corrected, if necessary, using the extrapolation technique described in Chapter 5) is used as a source across the center of the aperture in the Stage Two models.

The results of several tests are presented in this chapter which demonstrate that the electric field at the center of an aperture, as determined by FDTD in the stage-one model, can appropriately be used

as the excitation source at the center of an aperture in the MoM model of stage two. This is shown to be true since the field distribution in the modeled aperture is the same using either FDTD or MoM.

The investigation presented in this chapter with MoM looks at the same configurations studied in Chapter 4 for FDTD where an electrically large metal sheet with a single aperture is modeled. This allows comparisons with the original FDTD model, and eliminates any potential effects from the enclosure's physical dimensions or other environmental effects. The initial single aperture model is then extended to include multiple apertures in an infinite ground plane. In the next chapter, the hybrid technique is expanded to include a finite sized shielded enclosure with an aperture and the required test environment.

7.2 Initial Aperture Models

Creating an infinite metal plane with an aperture using the MoM technique is not as practical as in the FDTD technique. In order to simulate an infinite metal plane, a single, electrically large, wire mesh plate is created. Wire mesh can be used successfully to simulate a solid plane [39][40], especially when another wire is to be connected to the structure, as is discussed below. The wire mesh should be small compared to the wavelength of interest in order to insure the currents flow over the sheet as if it was a solid sheet of metal.

7.2.1 Single Aperture MoM Model

A 10 mm by 2 mm aperture is modeled as a hole in the wire mesh of a large plate using the MoM technique. Since it is desired for the model to be accurate to about 15 GHz (the first resonant frequency of this size aperture), the segment sizes are selected to be no larger than about 2 mm for

the MoM model. Figure 7.1 shows this wire mesh model. The radial wires at the corners and sides are used to increase the effective size of the plate to simulate an infinite plate.

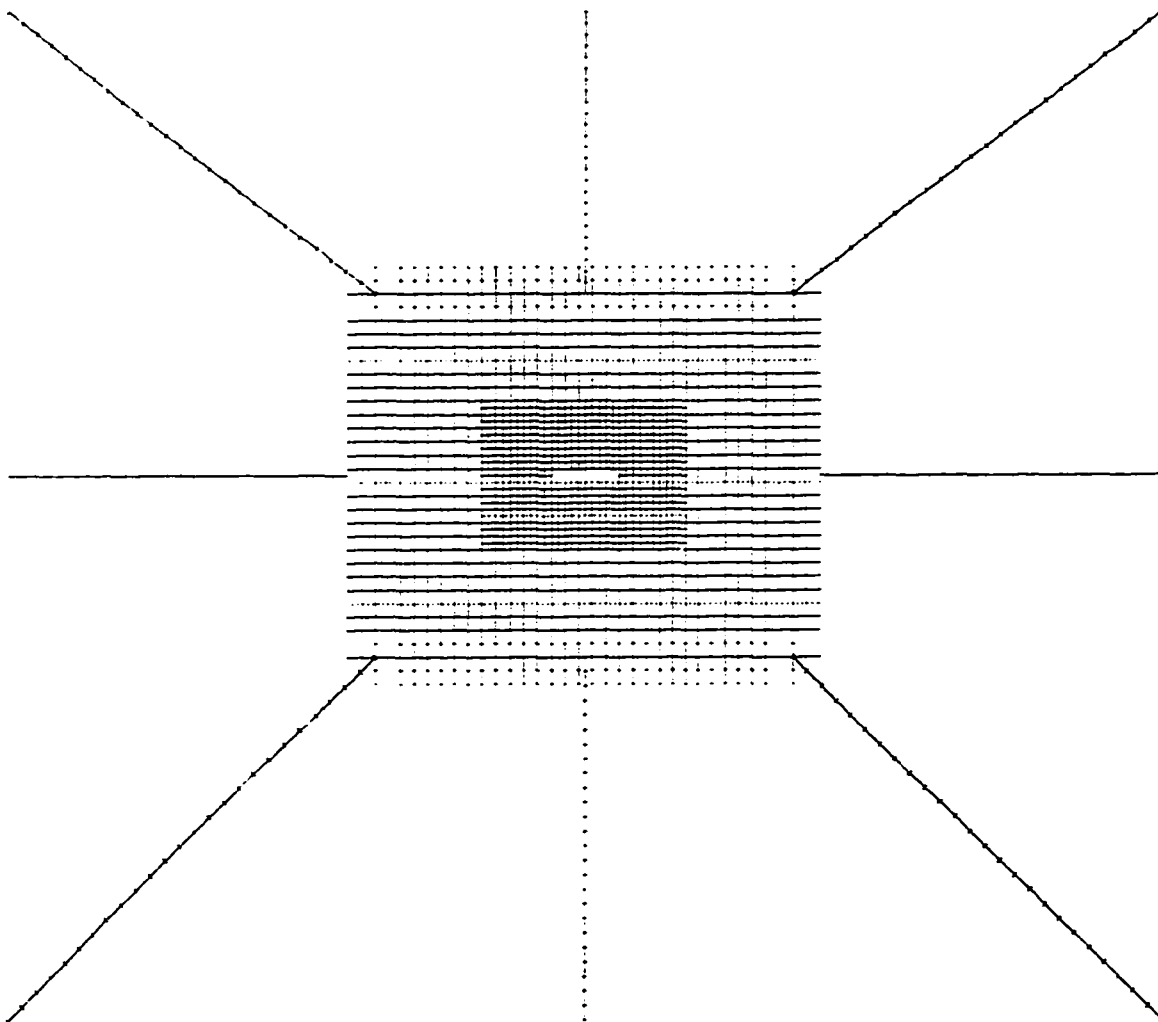


Figure 7. 1 MoM Wire Frame Model with Single 10x2 mm Aperture

The original FDTD 10 mm by 2 mm aperture problem is repeated with a larger computational domain in the outside area. The electric field level at a distance of 65 mm away from the aperture is found using FDTD. This distance is selected to create a reasonably-sized FDTD computational

domain while allowing the fields to be found in the far field at frequencies above about 770 MHz (one-sixth lambda from the aperture to the observation point).

The electric field level is found in the aperture in the Stage One Model and then is corrected at low frequencies using the Herzian dipole impedance method. The corrected electric field is then used as the voltage source across the aperture in the MoM (Stage Two) model. A single electric field source is placed across the center of the aperture and set to the maximum value (center location) of the Stage One model results. The electric field distribution within the aperture is very similar to the FDTD models, and the results are shown in Figure 7.2. The radiated electric field results are compared in Figure 7.3, and show a good agreement between modeling techniques between about 4 - 15 GHz, thus validating the use of MoM as a second stage in the hybrid approach to modeling apertures

The lower frequencies (typically below 4 GHz) in the FDTD model results may be affected by the absorbing boundary condition. Since it is not always practical to increase the FDTD computational domain to a point where there are no ABC effects, the results in the FDTD case may be limited in that the low frequency information may be in error. However, since the hybrid FDTD/MoM model results at those same low frequencies use the corrected aperture fields (from the techniques discussed in Chapter 5), the hybrid FDTD/MoM results show the correct low frequency electric field values.

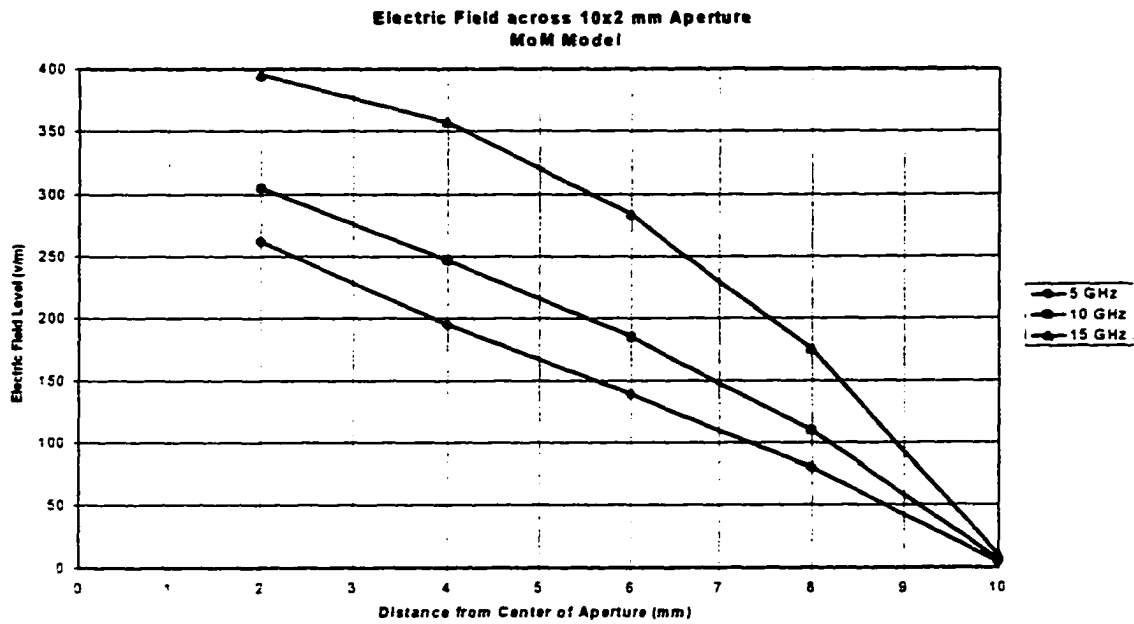


Figure 7. 2 Electric Field Distribution from MoM Model for 10x2 mm Aperture

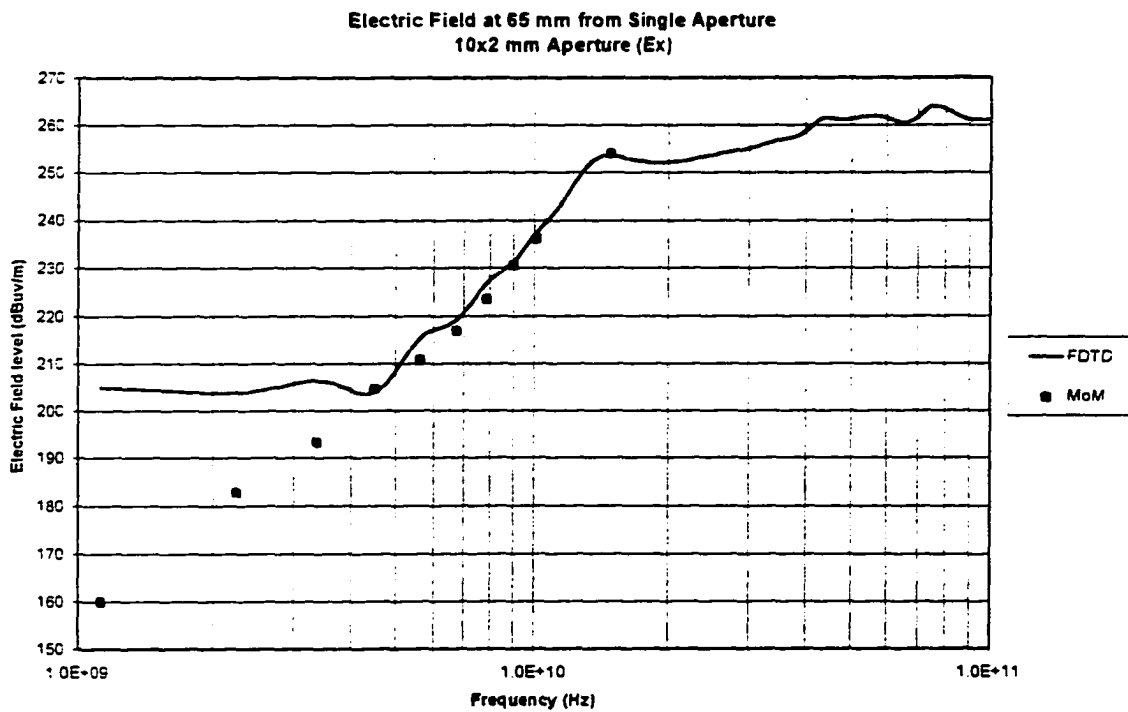


Figure 7. 3 Comparison Between MoM and FDTD at 65mm from Single Aperture

7.2.2 Double Aperture MoM Model

The above effort is now repeated for the case of two side-by-side 10 mm by 2 mm apertures, separated by only 2 mm. Practical experience has shown that closely spaced apertures are more likely to interact than apertures spaced relatively far apart. A MoM wire mesh model was developed to include two apertures on an electrically large metal plate, and is shown in Figure 7.4. Electric field sources are placed across both apertures, and set to the level determined from the Stage One model, and corrected using the Herizian dipole impedance technique. The radiated field levels at the same location (65 mm away from the apertures) are shown in Figure 7.5 from both the FDTD-only and hybrid FDTD/MoM models, and again show good agreement between the techniques between 3 - 15 GHz. The lower frequencies (below 3 GHz) in the FDTD model results are affected by the absorbing boundary condition. As in the single aperture case, the hybrid FDTD/MoM model results at those same low frequencies use the corrected aperture fields (from the techniques discussed in Chapter 5), and therefore show the correct low frequency electric field values. This again demonstrates the importance of modifying the aperture fields at low frequencies, and the importance of using this two stage hybrid modeling approach.

It is apparent from Figures 7.3 and 7.5 that the two modeling techniques agree over a limited frequency range very well. The limitation on the agreement at low frequencies is not due to the MoM model or the hybrid technique, but rather the FDTD model. As mentioned earlier, the FDTD absorbing boundary must be placed at a greater distance than the one used in order to provide higher accuracy. Unfortunately, this necessitates enlarging the computational domain to a size which can be very impractical. The hybrid FDTD/MoM results are more reliable at lower frequencies, since there is no comparable boundary condition problem.

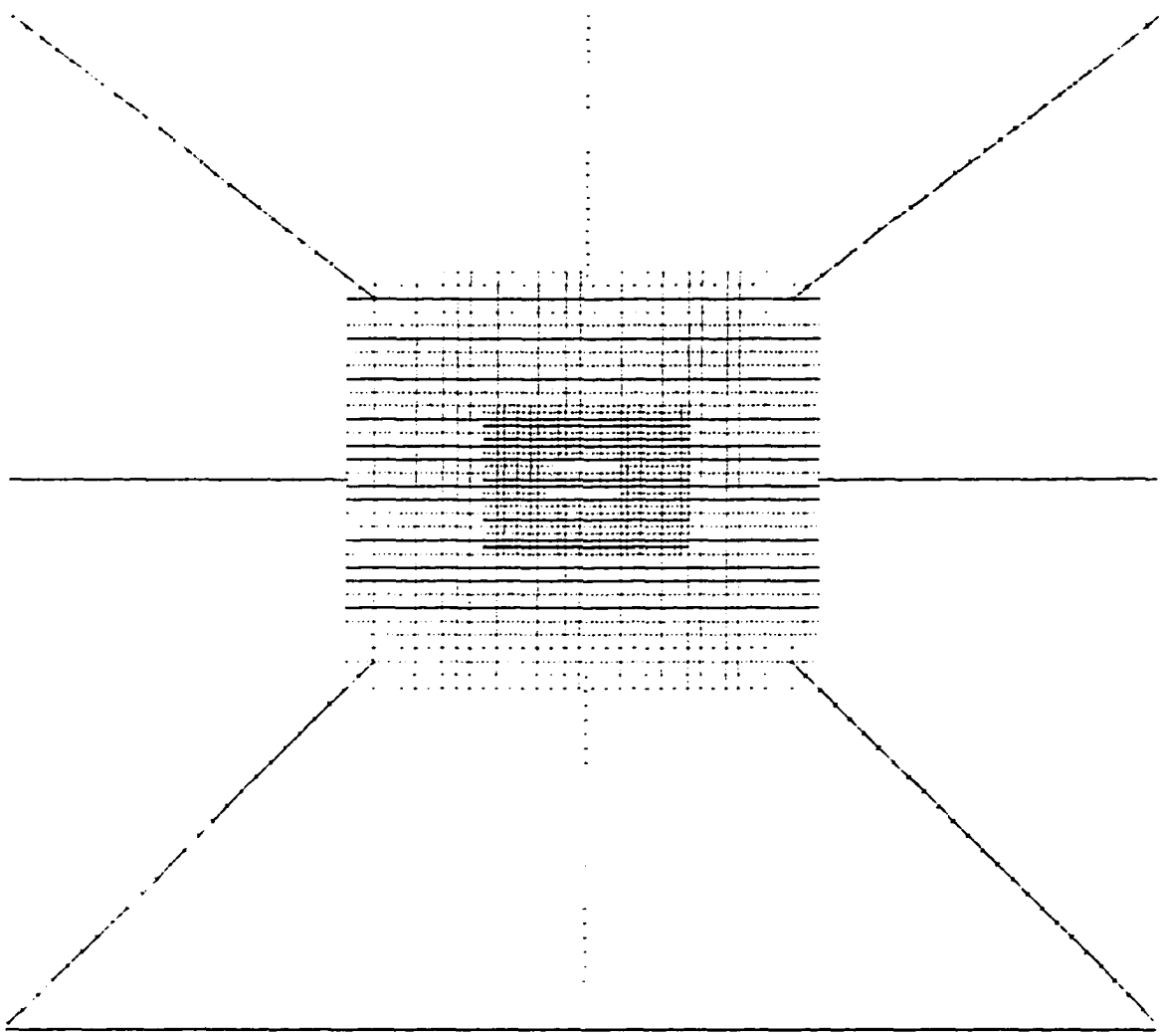


Figure 7. 4 MoM Wire Frame Model with Two 10x2 mm Apertures

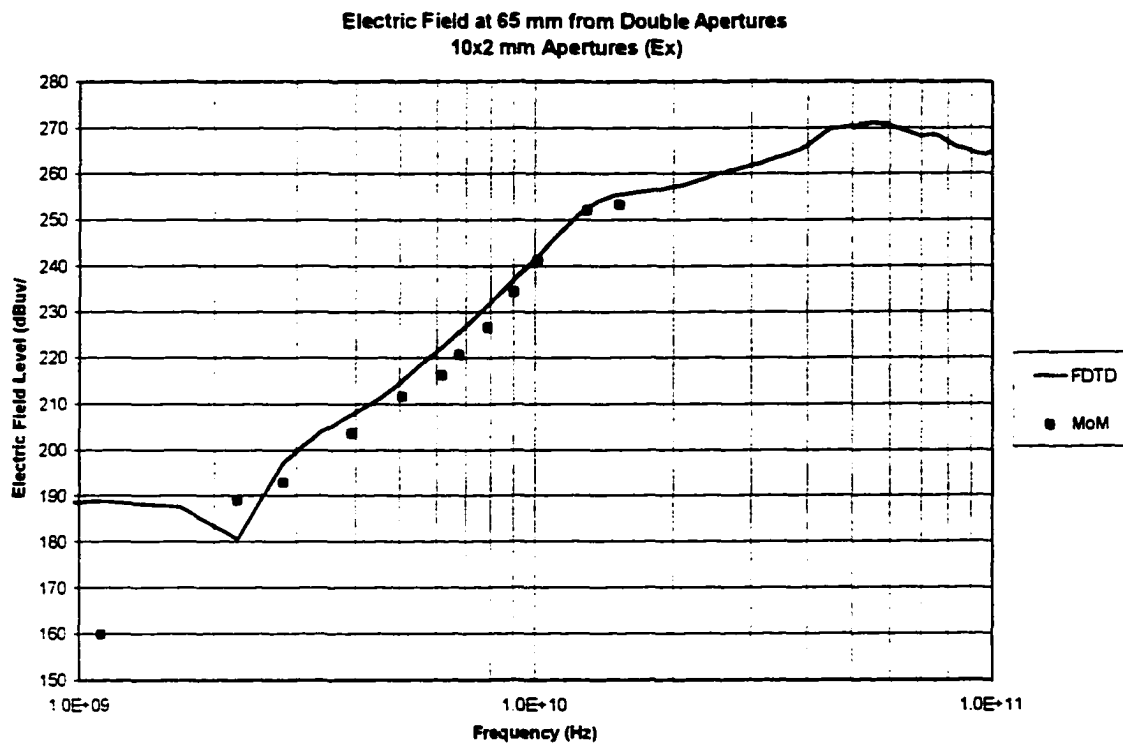


Figure 7. 5 Comparison Between MoM and FDTD at 65mm from Two Apertures

7.3 Summary

Comparisons between FDTD-only and Hybrid FDTD/MoM models for apertures in a metal plane show very good agreement over the range of frequencies where the FDTD-only model is valid (above the frequencies where the ABC introduces errors). The hybrid approach demonstrates its strength by improving upon the FDTD-only approach at low frequencies as described in Chapter 5. This chapter shows results which also validate the simplification of the electric field in the aperture from the entire

field distribution (found during the Stage One FDTD model) to a single electric field across the center of the aperture (for use by the Stage Two MoM model).

Hybrid models showing the effects of real-world test environment configurations demonstrate the importance of including these features in the model, and show how effectively the hybrid approach can include them.

CHAPTER 8

IMPLEMENTING THE HYBRID TECHNIQUE

8.1 Introduction

In this chapter, the hybrid technique is extended from a flat metal plate with apertures to three-dimensional shielded enclosures with apertures including long attached wires and the required test environment. The implementation of the hybrid technique is described in detail and an example showing the effects of including the long wires and test environment is given.

8.2 Detailed Description of the Hybrid Modeling Technique

The first step to use the hybrid modeling technique described here is to create the FDTD model of the enclosure, aperture(s), the internal source and whatever internal structure is considered important. In the case of an empty shielded enclosure (100 mm cube) with a 10 x 2 mm aperture, the FDTD cells must be small enough to describe the aperture correctly. For this example, a FDTD cell size of .5 mm is selected. This size is also small enough to provide at least 10 cells per wavelength up to the highest frequency of interest, as per FDTD approach requirements.

The source is selected to be a simple current on a wire. As described earlier, this is representative of a PCB ground reference plane edge. The wire is oriented perpendicular to the aperture to ensure maximum possible emissions coupled through the aperture.

Figure 8.1 shows a diagram of the FDTD model. The aperture is placed on the top face of the enclosure for convenience, but could be on any side desired. The top part of the enclosure is extended beyond the enclosure walls to restrict any external resonances from affecting the fields in the aperture. The internal structure of the enclosure is maintained to allow any internal resonances to occur. The FDTD simulation must be run long enough to ensure all the resonance effects have died down.¹ Both the electric and magnetic field at the center of the aperture is saved as the output from this Stage One model.

The time domain electric and magnetic field results are then converted to the frequency domain using a Fast Fourier Transform (FFT). The frequency domain impedance (E/H) is examined to determine if errors occurred due to the ABC's close proximity to the aperture at low frequencies which are of interest. The electric field is then corrected using the Herzian dipole technique described in Chapter 5.

The enclosure is modeled in MoM for Stage Two using a wire mesh frame with the openings in the wire mesh small compared to the shortest wavelength of interest. The corrected electric field is then applied across the center of the aperture in the MoM model for each frequency desired.

¹ The length of time needed to allow the resonances to die down depends on the Q-factor of the enclosure. The use of non-perfect conductivities [33] for the enclosure walls will greatly reduce the Q-factor of the enclosure and provide more realistic results.

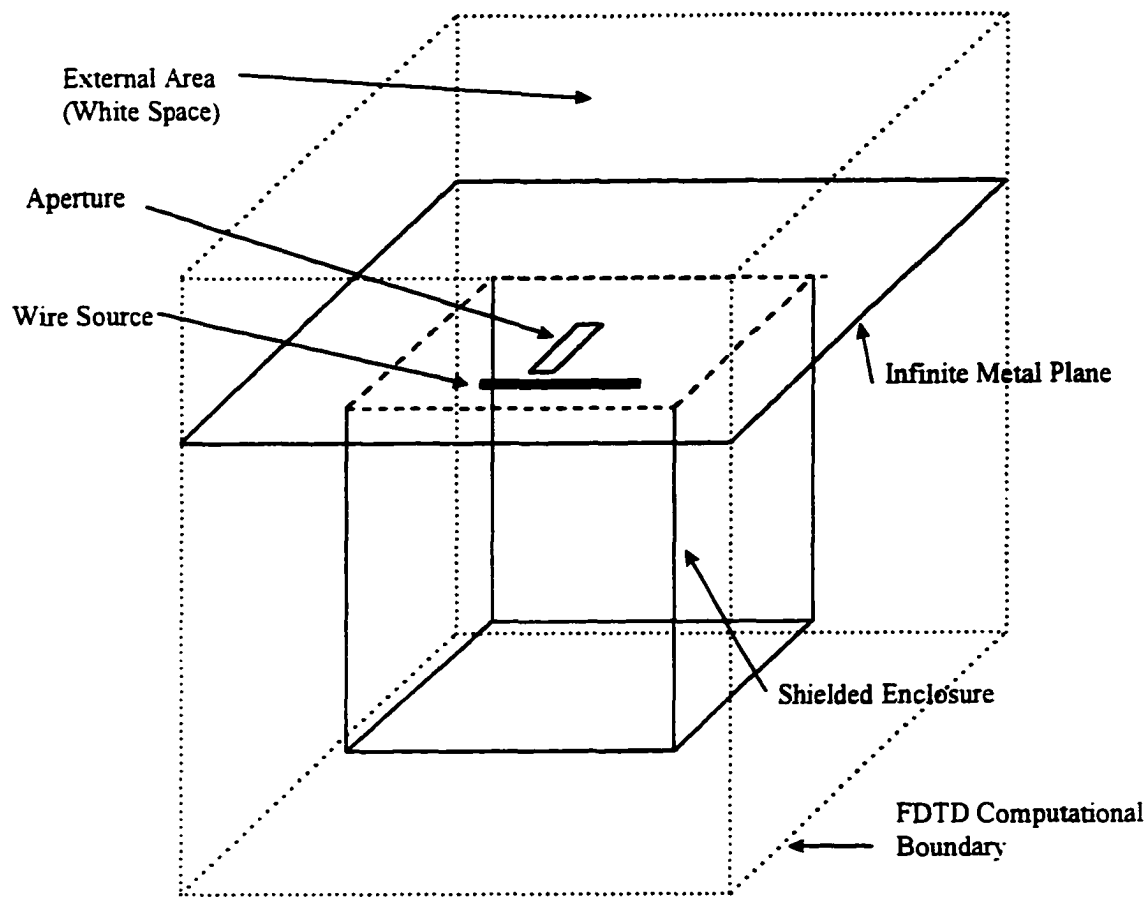


Figure 8. 1 FDTD Example Model of Shielded Enclosure and Aperture

8.3 Enclosed Shielded Enclosure with Aperture Model

An example is presented to show the usefulness of the hybrid technique. A shielded enclosure with a size of 100 mm cubed and a 10 mm by 2 mm aperture on the front side of the enclosure is used to demonstrate this technique. The enclosure size is selected to insure that any physical size effects will be observed, and that the enclosure's dimensions will not appear as an infinite plane to the aperture at the frequencies of interest. Figure 8.2 shows a diagram of the wire frame enclosure model used for MoM second stage models.

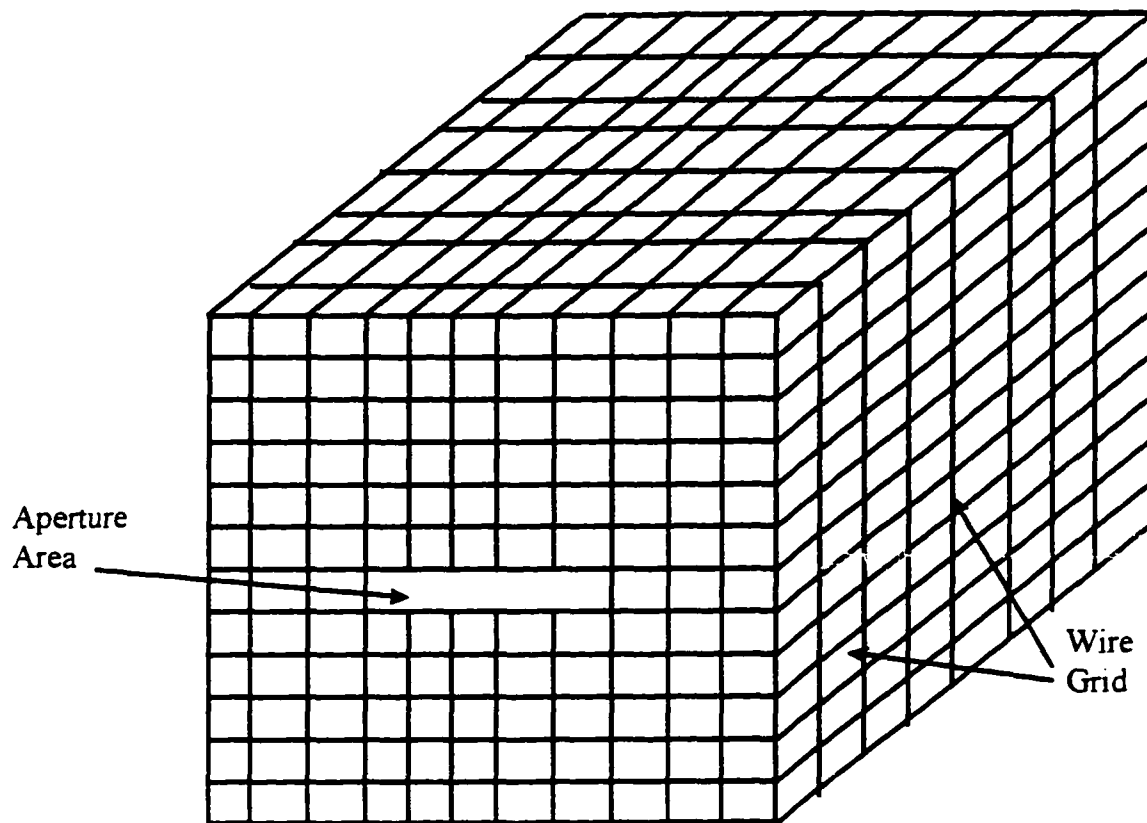


Figure 8. 2 MoM Wire Frame Enclosure Model

The (corrected) electric field in the center of the aperture from the Stage One model is then applied across the center of the MoM aperture and MoM used to find the fields at a 10 meter distance from the aperture.

8.3.1 Hybrid Model Comparison Between Free Space and Real-World Test Environment

As stated earlier, it is important to model the test environment correctly. The following examples demonstrate the effects of the environment on the final results. As mentioned in Chapter 1, EMI emissions measurements are required to be made over a ground plane. The receive antenna must be 10 meters away, and it must be scanned (for maximum receive level) over a one to four meter

height while rotating 360 degrees. The scanning of the antenna height ensures there is no chance of a destructive interference path artificially lowering the measured emissions levels. The rotation of the EUT through the 360 degrees ensures the maximum emissions are received, regardless of any possible directionality of the EUT's radiation pattern.

Figures 8.3 and 8.4 show the model results for the shielded enclosure EUT with and without the ground plane present for both the horizontal and vertical polarizations. The presence of the ground plane, and the effect of scanning over the height range, can greatly increase the measured emissions level due to the reflected wave adding in phase to the direct wave.

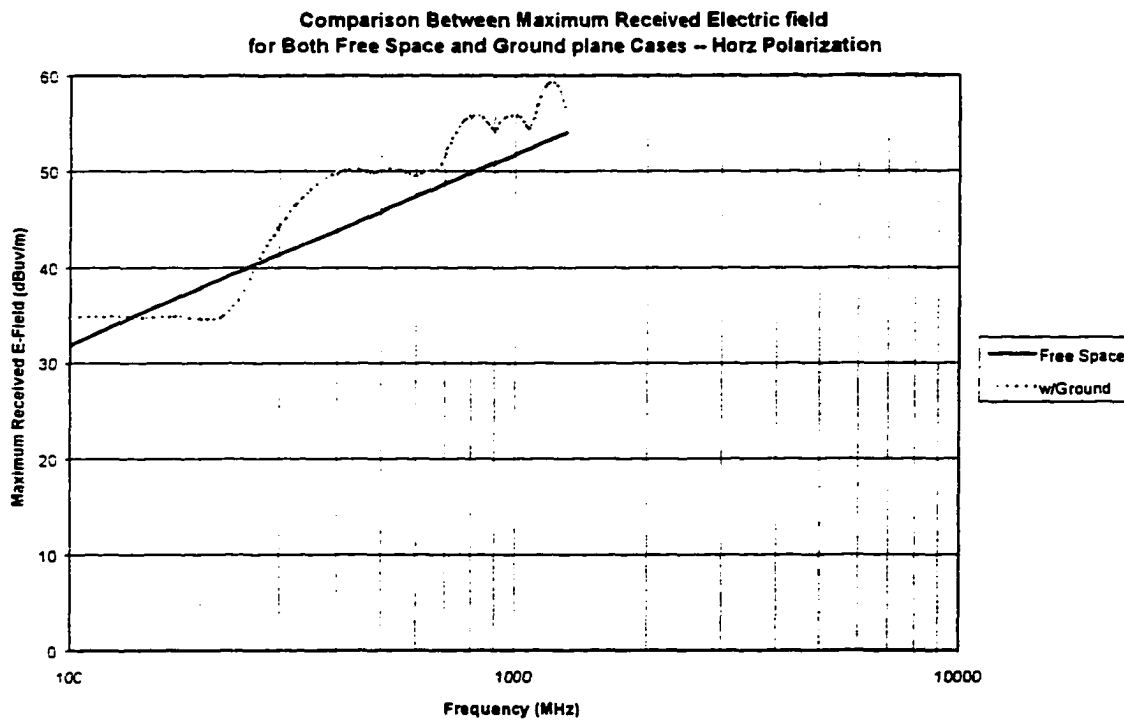


Figure 8. 3 Maximized Electric Field Comparison with and without Ground Plane (Horizontal Polarization)

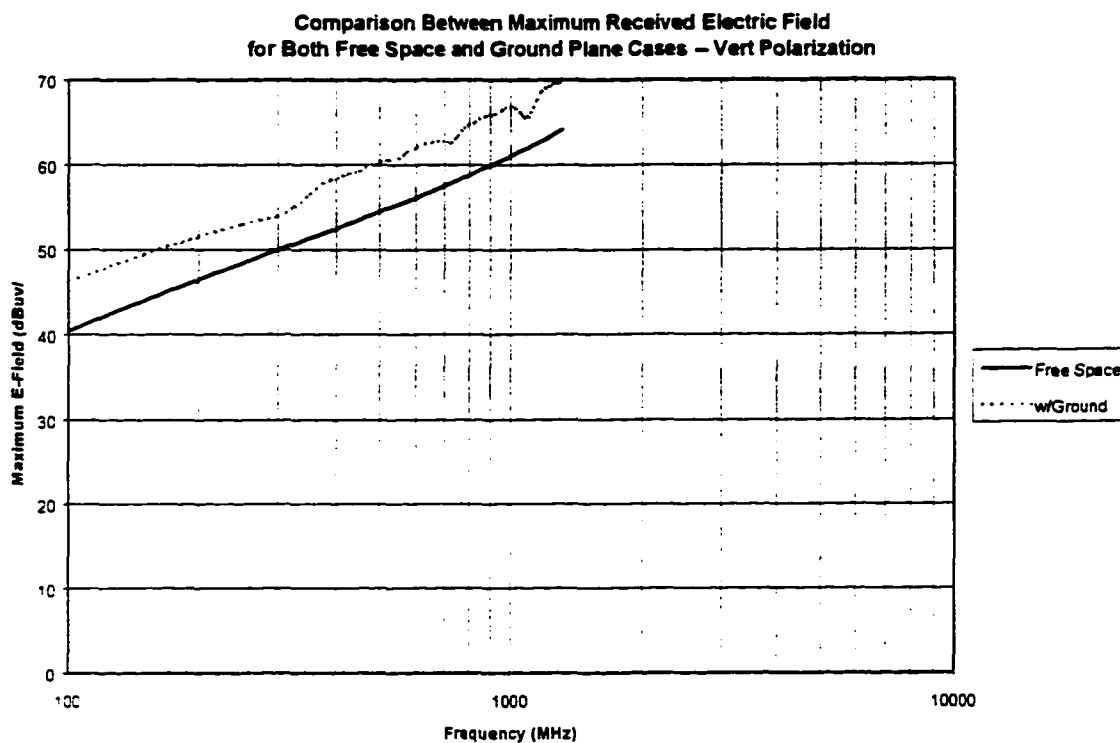


Figure 8. 4 Maximized Electric Field Comparison with and without Ground Plane (Vertical Polarization)

EMI Emissions test standards also require that all cables be attached to the EUT. This effectively increases the EUT's electrical size, and typically increases the emissions levels significantly at some frequencies. A single cable, one meter long, is now attached to the initial enclosure model, as shown in Figure 8.5. This cable is attached directly to the enclosure shield, as in the case of a cable shield being 'grounded' to the case.

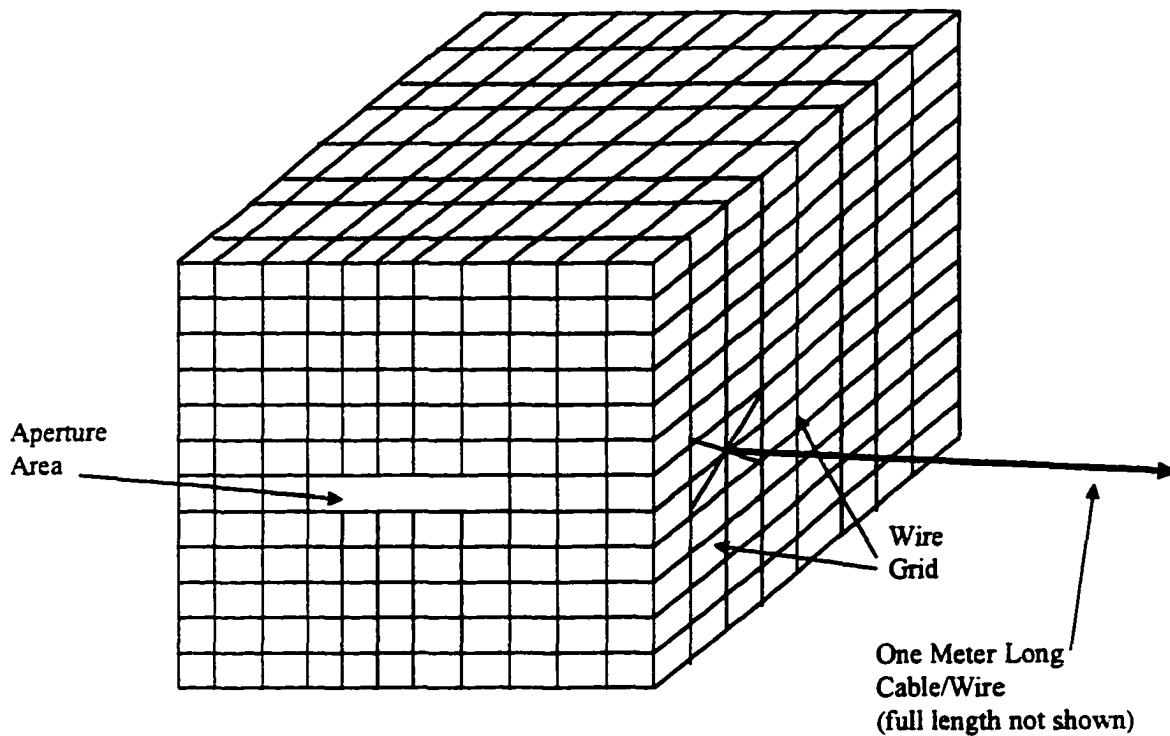


Figure 8. 5 MoM Model of Shielded Enclosure with 1 meter Cable Attached

The same electric field is applied across the aperture for this new configuration. The maximum received emissions are greatly increased, as seen in Figure 8.6, due to the addition of the cable. This demonstrates the importance of the hybrid model including all of the test environment features.

8.4 Summary

This chapter provides a description of the implementation process for the hybrid technique. An example is provided to show how to create the Stage One FDTD model of a shielded enclosure as well as the Stage Two MoM model of the same enclosure. The example provides results showing significant impact the attached wire and the measurement environment has on the final results of the model.

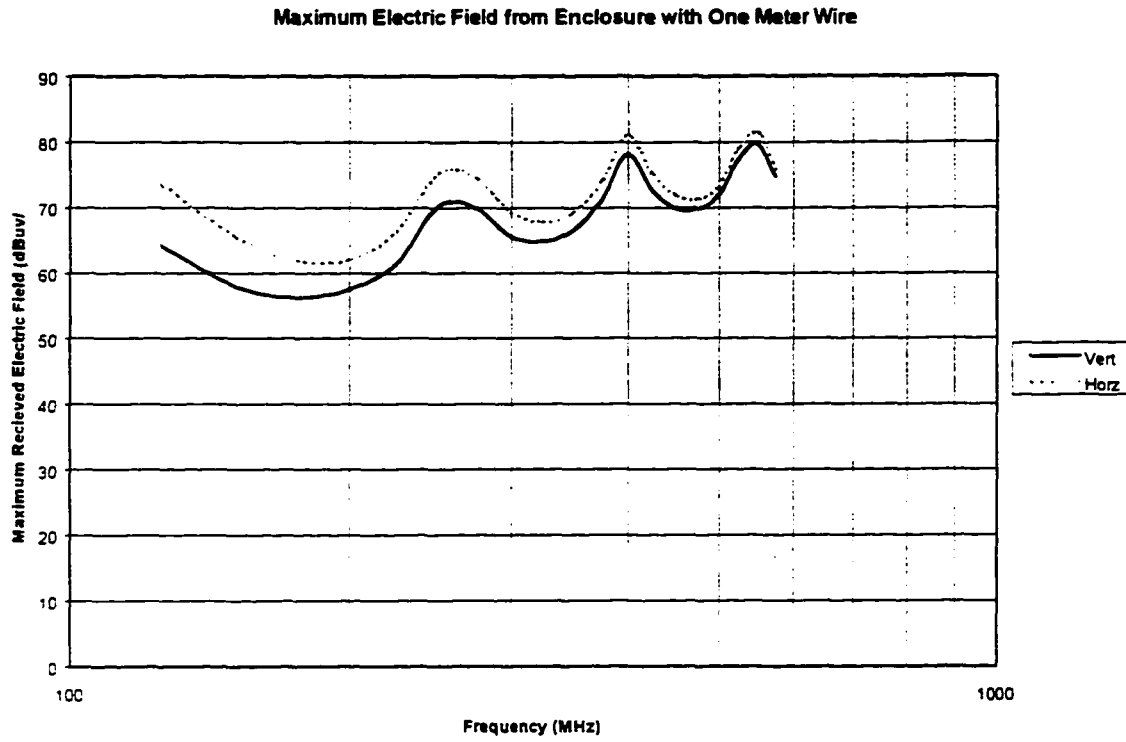


Figure 8. 6 Maximum Received Electric Field from EUT with One Meter Wire Attached

CHAPTER 9

SUMMARY

A hybrid FDTD/MoM approach has been shown to allow EMI modeling of emissions from PCB sources inside a shielded enclosure with apertures, including the required equipment configuration and test environment. This approach allows modeling of a complex problem that has been previously impractical to model. Using this hybrid approach, engineers can now predict the pass/fail performance of a product against national and international EMI regulatory requirements.

The hybrid approach uses FDTD as the Stage One model to find the field in the aperture or apertures in a shielded enclosure due to a source within the enclosure and any internal enclosure features. The actual source can be whatever is considered to be the important source of EMI energy by the engineer. In this dissertation, the source is assumed to be the current along the edge of a PCB reference plane due to a microstrip on the PCB. Regardless of the source selected, the Stage One model determines the field within the aperture due to that source, the geometry of the enclosure, and the distance to the aperture.

A detailed study of the field distribution throughout the aperture using the aperture impedance showed the variation of the field across the aperture under various conditions. The maximum field strength remained in the center of the aperture regardless of the source position and distance when the frequency was limited to wavelengths longer than twice the aperture length.

At low frequencies, where the constraints of the ABC are often violated in practical FDTD models (due to the electrically close proximity of the aperture to the computational boundaries), errors often occur in the aperture field. The impedance and the electric field level at low frequencies can be corrected using the Herzian dipole impedance technique described in Chapter 5.

The corrected aperture fields are then used as a source for the second stage models using the MoM technique. Wire frame mesh models of electrically large metal plates with apertures are used to validate the hybrid approach against the FDTD-only approach and showed good agreement where the FDTD results are not contaminated by the absorbing boundary condition proximity.

The hybrid approach was then extended to model finite-sized enclosures with apertures. Long attached wires are included, and the effects of the test environment ground plane is demonstrated. Results are presented that include low frequencies where the FDTD fields are corrected, as well as frequencies where no correction is required. The final results from the hybrid approach can be directly compared to emission limits set by EMI regulations.

Suggestion for Future Work

This dissertation is restricted to frequencies where the aperture was smaller than one-half wavelength long. This is a reasonable limitation, since design engineers know that little shielding occurs when apertures are equal to, or greater than, one-half wavelength. Future work might investigate how this limitation could be eliminated, and more accurate modeling performed at these higher frequencies.

All apertures in this effort were long thin apertures. Future work could examine how to implement this hybrid technique for wide apertures. For wide apertures it is expected that a MoM model of a patch antenna must be used to determine the correct impedance at low frequencies, in place of the Herzian dipole impedance approach used for long thin apertures.

Other future work could include a wire through an aperture. The use of a Surface Impedance Boundary condition (SIBC) [27][28] to model the impedance of the aperture with the wire could possibly allow the effect of long external wires to be included in the FDTD model.

REFERENCES

- [1] U.S. Code of Federal Regulations, Title 47, part 15, subpart J.
- [2] CISPR-22. International Electrotechnical Commission, "Limits and methods of measurement of radio interference characteristics of information technology equipment," 1995-04
- [3] B.R Archambeault, "Modeling of EMI Emissions from Microstrip Structures with Imperfect Reference Planes," *Applied Computational Electromagnetics Society Symposium*, March 1997, pp. 1058-1063.
- [4] S. Poh. "Electromagnetic Emissions from Microstrip Discontinuities in Interchip Packaging." Internal Digital Equipment Corporation Report. 13 Feb 91.
- [5] S. Daijavad, H. Heeb. "On the Effectiveness of Decoupling Capacitors in Reducing Electromagnetic Radiation from PCBs." *1993 IEEE International Symposium on Electromagnetic Compatibility*, pp. 330-333.
- [6] B.R. Archambeault. C. Brench, "Shielded Air Vent Designs Guidelines from EMI Modeling." *1993 IEEE International Symposium on Electromagnetic Compatibility*, pp. 195-199.
- [7] D.M. Hockanson. J.L. Drewniak. T.H. Hubing. T.P. VanDoren, "Application of the Finite Difference Time Domain Method to Radiation from Shielded Enclosures." *1994 IEEE International Symposium on Electromagnetic Compatibility*, pp. 83-88.
- [8] B.L. Brench. C.E. Brench, "Shield Degradation in the Presence of External Conductors." *1994 IEEE International Symposium on Electromagnetic Compatibility*, pp. 269-273.
- [9] B.R. Archambeault. C.E. Brench. "Modeled and Measured Results from Two Proposed Standard EMI Modeling Problems." *1995 IEEE International Symposium on Electromagnetic Compatibility*, pp. 349-352
- [10] B. R. Archambeault and K. Chamberlin, "Modeling the EMI Performance of Various Seam Shapes". *Applied Computational Electromagnetics Society International Symposium*, 1995
- [11] J.L. Drewniak, T.H. Hubing, T.P. Van Doren, "Investigation of Fundamental Mechanisms of Common-Mode Radiation from Printed Circuit Boards with Attached Cables, Internal Report, University of Missouri-Rolla.
- [12] T.H. Hubing and J.K. Kaufman, "Modeling the Electromagnetic Radiation from Electrically Small Table-Top Products," *IEEE Transactions on Electromagnetic Compatibility*, Vol. 31, No. 1, pp. 74-84, Feb 89.
- [13] P. Harms. R. Mittra, and J. Nadolny, "Simulating Measurements for a Cable Radiation Study." *IEEE Transactions on Electromagnetic Compatibility*, Vol. 38, No. 1, pp. 25-31, Feb. 96

- [14] C.A. Balanis. *Advanced Engineering Electromagnetics*, Wiley, 1989, Sect. 7.8.
- [15] R.F. Harrington. *Time-Harmonic Electromagnetic Fields*, McGraw-Hill Book company, 1961.
- [16] C.M. Butler, Y. Rahmat-Samii, and R. Mittra, "Electromagnetic Penetration Through Apertures in Conducting Surfaces," *IEEE Transactions on Antennas and Propagation*, vol. AP-26, No. 1, pp. 82-93, Jan 1978.
- [17] R.F. Harrington and J.R. Mautz, "A Generalized Network Formulation for Aperture Problems." Lecture #8, *Lectures on Computational Methods in Electromagnetics*, The SCEEE Press. 1981.
- [18] C.M. Butler. "Investigation of a Scatterer Coupled to an Aperture in a Conducting Screen." *IEE Proceedings*, vol.127, pp. 161-169, June 1980.
- [19] R.F. Harrington and D.T. Auckland. "Electromagnetic Transmission Through Narrow Slots in Thick Conducting Screens." *IEEE Transactions on Antennas and Propagation*, vol. AP-28, No.5 pp. 616-622, Sept 1980.
- [20] R.F. Harrington. "Resonant Behavior of a Small Aperture Backed by a Conducting Body." Lecture #10, *Lectures on Computational Methods in Electromagnetics*, The SCEEE Press. 1981.
- [21] C.M. Butler. "A Review of Electromagnetic Diffraction by Small Apertures in Conducting Surfaces." Lecture #7, *Lectures on Computational Methods in Electromagnetics*, The SCEEE Press. 1981
- [22] Yee. K. S., "Numerical Solution of Initial Boundary Value Problems Involving Maxwell's Equations in Isotropic Media," *IEEE Trans. Antennas and Propagation*, vol. 14, 1966, pp.302-307.
- [23] Taflove. A., K. R. Umashankar, B. Beker, F. A. Harfoush, and K. S. Yee, "Detailed FD-TD Analysis of Electromagnetic Fields Penetrating Narrow Slots and Lapped Joints in Thick Conducting Screens." *IEEE Trans. Antennas and Propagation*, vol. 36, 1988, pp.247-257.
- [24] Mur. G., "Absorbing Boundary Conditions for the Finite-Difference Approximation of the Time-Domain Electromagnetic Field Equations," *IEEE Trans. Electromagnetic Compatibility*, vol. 23, 1981, pp. 377-382.
- [25] Higdon. R. L., "Absorbing Boundary Conditions for Difference Approximations to the Multi-dimensional Wave Equation," *Mathematics of Computation*, vol. 47, 1986, pp. 437-459.
- [26] Liao. Z. P., H. L. Wong, B. P. Yang, and Y. F. Yuan, "A Transmitting Boundary for Transient Wave Analyses," *Scientia Sinica (series A)*, vol. XXVII, 1984, pp. 1063-1076.
- [27] A. Taflove, *Computational Electrodynamics. The Finite-Difference Time-Domain Method*, Artech House. 1995.

- [28] K.S. Kunz and R.J. Luebbers. *The Finite Difference Time Domain Method for Electromagnetics*. CRC Press, 1993.
- [29] Ramahi, O. M.. "Complementary Operators: A method to annihilate artificial reflections arising from the truncation of the computational domain in the solution of partial differential equations." *IEEE Trans. Antennas and Propagation*, Vol. 43, No. 7, July 1995.
- [30] Ramahi, O. M.. "Application of the complementary operator method to the finite-difference-time-domain solution of the three-dimensional radiation problem." *Microwave and Optical Technology Letters*, Vol. 9, No. 3, June 1995.
- [31] Berenger, J.-P.. "A perfectly matched layer for the absorption of electromagnetic waves," *J. Computational Physics*, vol. 114, 1994, pp. 185-200.
- [32] R. Luebbers and C. Penny. "Scattering from Apertures in Infinite Ground Planes using FDTD." Pennsylvania State University Internal Report, Feb 1993.
- [33] K. Chamberlin and L. Gordon. "Modeling Good Conductors Using the Finite-Difference Time-Domain Technique." *IEEE Trans. Electromagnetic Compatibility*, vol. 37, No. 2, May 1995.
- [34] J.D. Kraus. *Antennas*. McGraw-Hill Book Company, Second Edition 1988
- [35] C.T.A. Johnk. *Engineering Electromagnetic Fields and Waves*. Wiley, 1988
- [36] R.F Harrington. *Field Computation by Moment Methods*. Krieger Publishing Company, 1985
- [37] T.H. Hubing. "Modeling the Electromagnetic Radiation from Electrically Small sources with Attached Wires." Ph.D. Dissertation. North Carolina State University, 1988
- [38] C.A. Balanis. *Advanced Engineering Electromagnetics*. Wiley, 1989, Sect. 12.4.1.
- [39] Ludwig, A. C.. "Wire grid modeling of surfaces," *IEEE Trans. Antennas and Propagation*, vol. AP-35, No. 9, September 1987, pp. 1045-1048
- [40] Archambeault, B. R.. R. Mellitz. "EMI Prediction using wire mesh boxes in NEC." *Applied Computational Electromagnetics Society Symposium*, March 1993.

APPENDIX A

**ADDITIONAL APERTURE SIZE
CHARACTERIZATION**

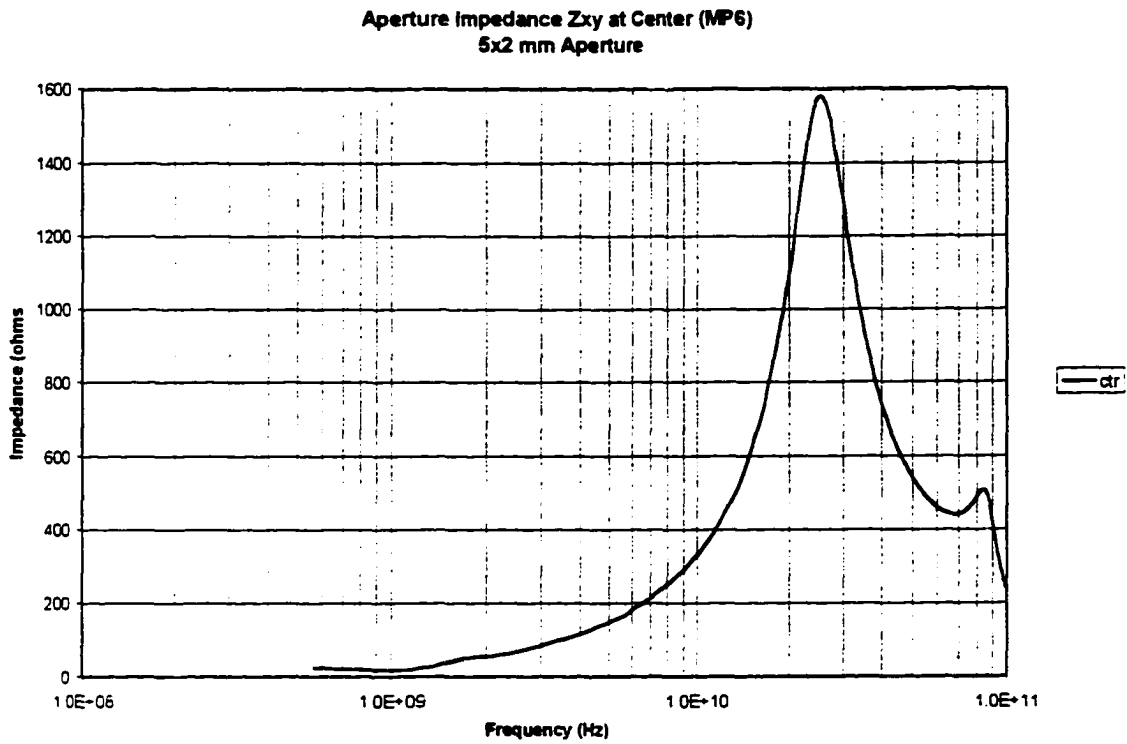


Figure A- 1 Z_{xy} Impedance at Center of 5x2 mm Aperture

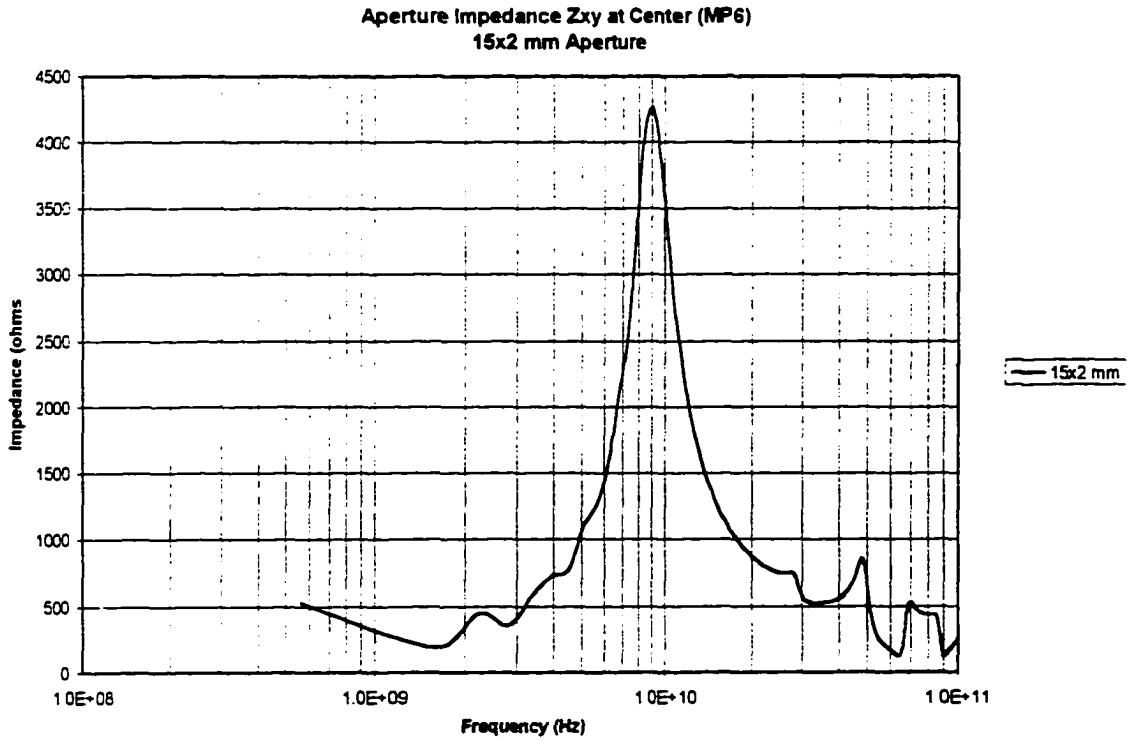


Figure A- 2 Z_{xy} Impedance at Center of 15x2 mm Aperture

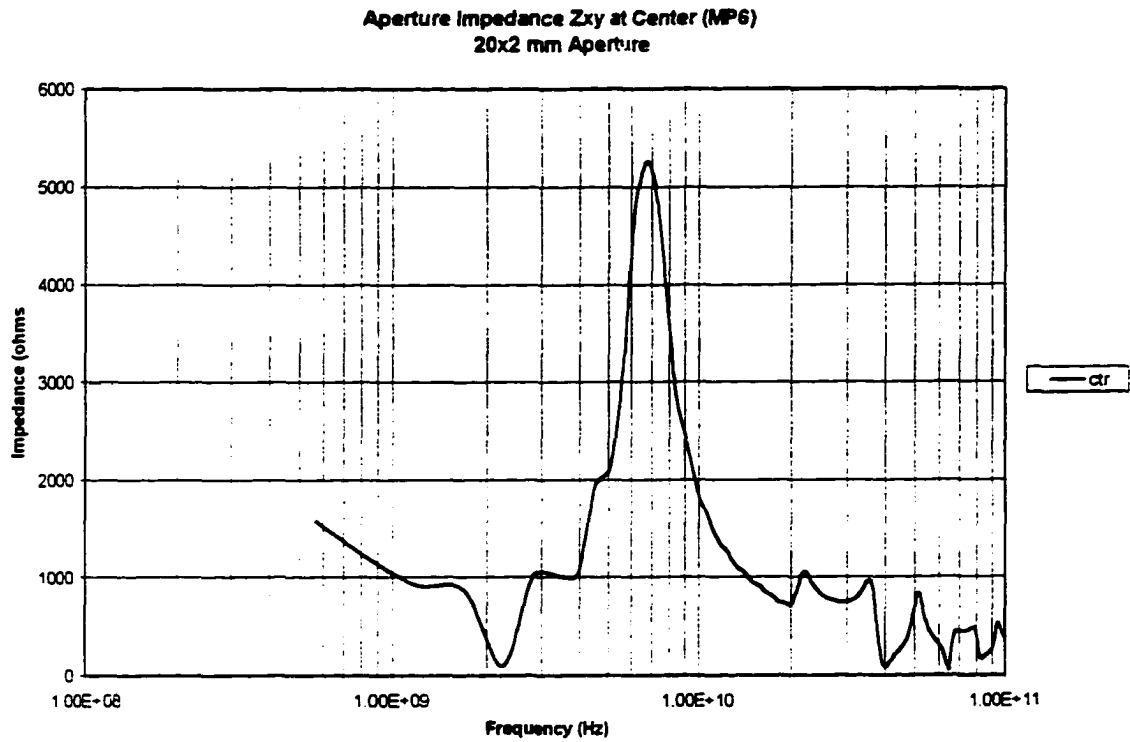


Figure A- 3 Z_{xy} Impedance at Center of 20x2 mm Aperture

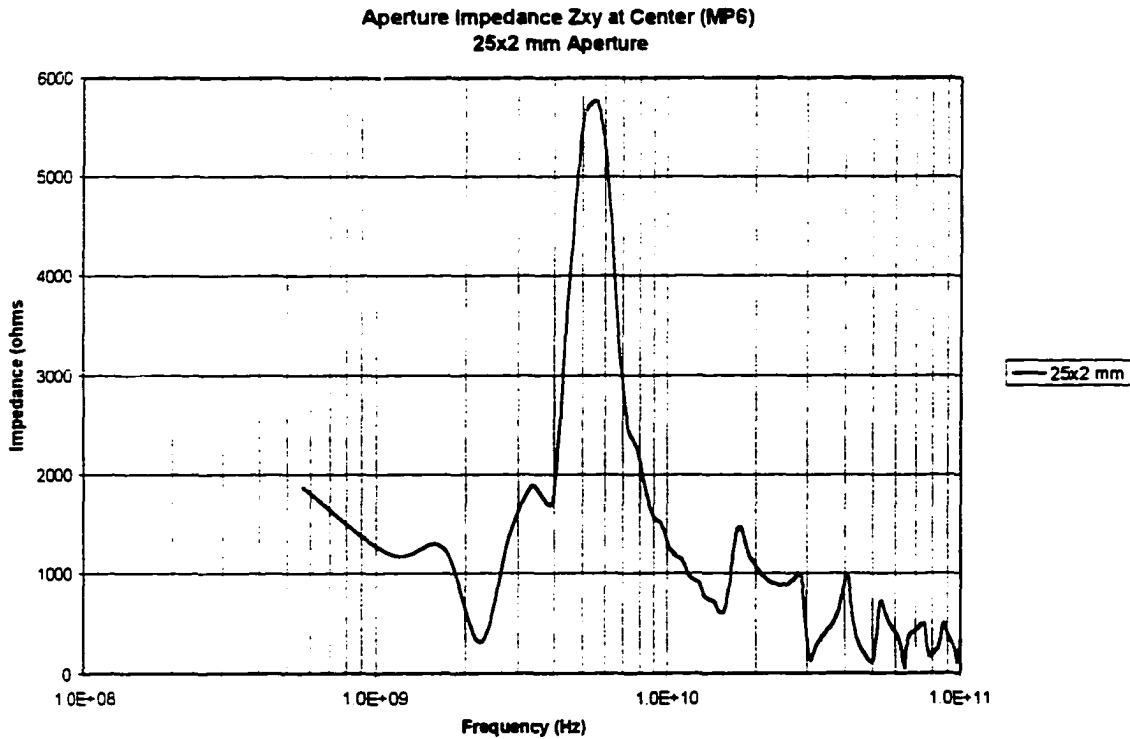


Figure A- 4 Z_{xy} Impedance at Center of 25x2 mm Aperture

Aperture Impedance (Z_{xy}) vs Position (5 x 2 mm Aperture)

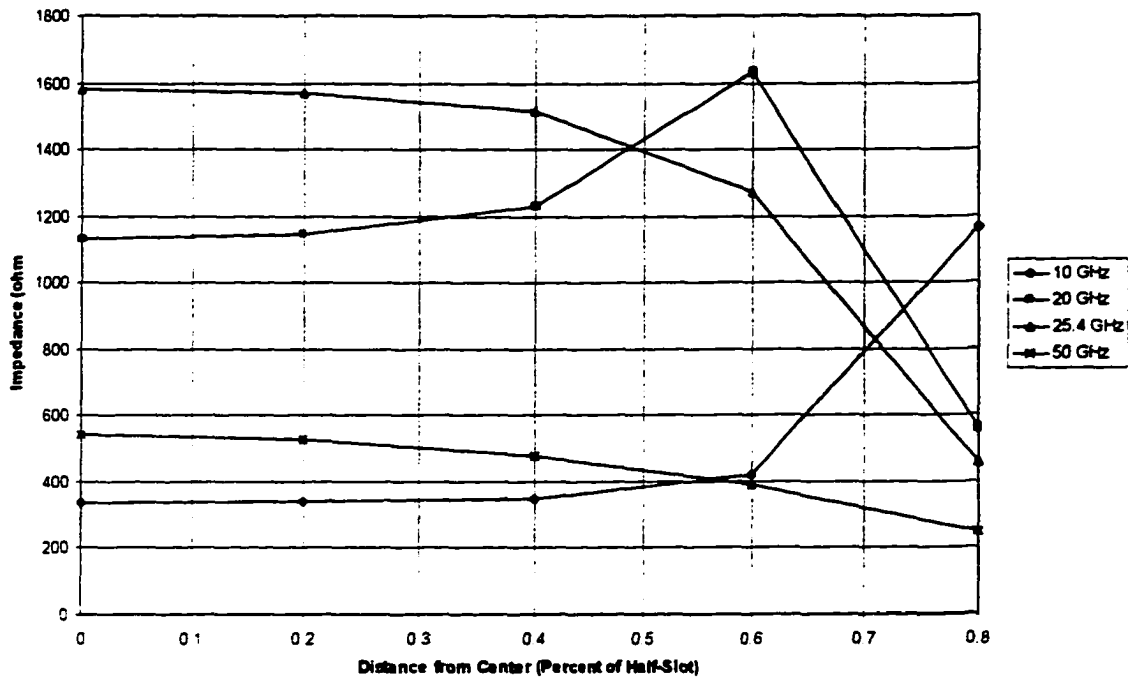


Figure A- 5 Variation of Impedance (Z_{xy}) Along Aperture (5x2 mm)

Aperture Impedance (Z_{xy}) vs Position (20x2 mm Aperture)

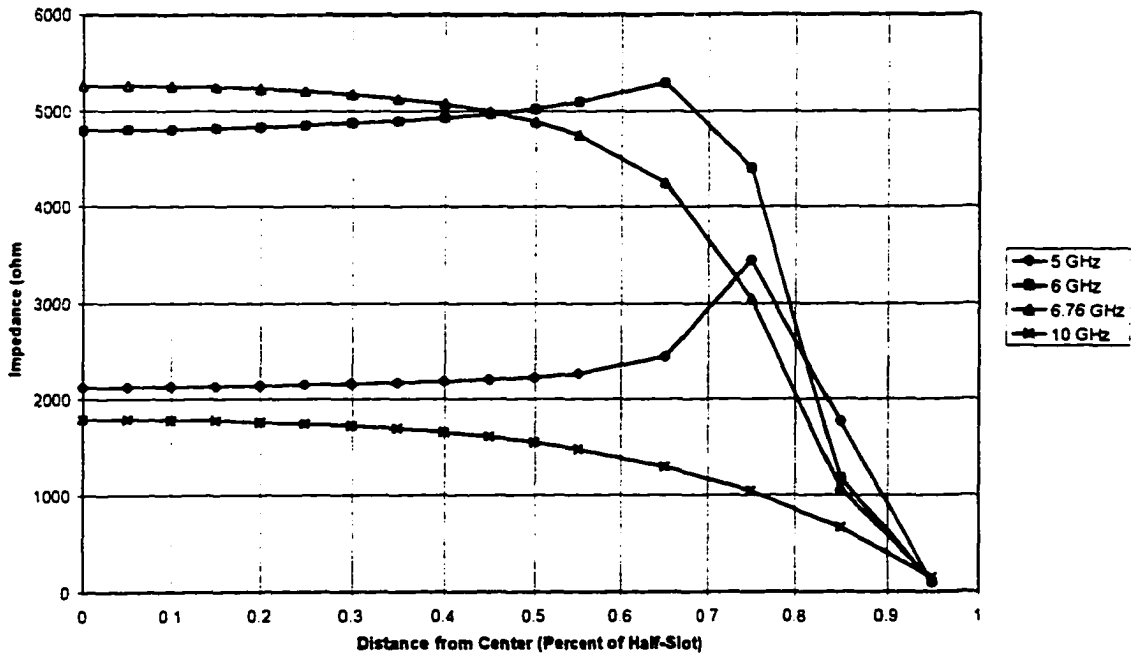


Figure A- 6 Variation of Impedance (Z_{xy}) Along Aperture (20x2 mm)